

---

# AdaNCA: Neural Cellular Automata As Adaptors For More Robust Vision Transformer

---

Yitao Xu Tong Zhang Sabine Süsstrunk

École polytechnique fédérale de Lausanne, Lausanne, Switzerland,  
{yitao.xu, tong.zhang, sabine.susstrunk}@epfl.ch

## Abstract

Vision Transformers (ViTs) have demonstrated remarkable performance in image classification tasks, particularly when equipped with local information via region attention or convolutions. While such architectures improve the feature aggregation from different granularities, they often fail to contribute to the robustness of the networks. Neural Cellular Automata (NCA) enables the modeling of global cell representations through local interactions, with its training strategies and architecture design conferring strong generalization ability and robustness against noisy input. In this paper, we propose **Adaptor Neural Cellular Automata** (AdaNCA) for Vision Transformer that uses NCA as plug-in-play adaptors between ViT layers, enhancing ViT’s performance and robustness against adversarial samples as well as out-of-distribution inputs. To overcome the large computational overhead of standard NCAs, we propose *Dynamic Interaction* for more efficient interaction learning. Furthermore, we develop an algorithm for identifying the most effective insertion points for AdaNCA based on our analysis of AdaNCA placement and robustness improvement. With less than a 3% increase in parameters, AdaNCA contributes to more than 10% absolute improvement in accuracy under adversarial attacks on the ImageNet1K benchmark. Moreover, we demonstrate with extensive evaluations across 8 robustness benchmarks and 4 ViT architectures that AdaNCA, as a plug-in-play module, consistently improves the robustness of ViTs.

## 1 Introduction

Vision Transformers (ViTs) exhibit impressive performance in image classification through globally modeling token interactions via self-attention mechanisms [11, 14, 76]. Recent works show that integrating local information into ViTs, *e.g.*, using region attention [25, 37, 38, 53, 64, 69, 72] or convolution [8, 10, 16, 21, 22, 36, 41, 51, 67, 70, 74], further enhances the ViT’s capabilities in image classification. While advanced local structures contribute to better captures of local information, the robustness of ViTs has not increased. They remain vulnerable to noisy input such as adversarial samples [5, 9, 13, 40, 41] and out-of-distribution (OOD) inputs [17, 18, 27, 29, 66].

Recently, Neural Cellular Automata (NCA) has been proposed as a lightweight architecture for modeling local cell interactions [43], where cells are represented by 1D vectors. Similar to the idea of token interactions in ViTs, cells in NCA interact with each other by alternating between a convolution-based *Interaction* stage and an MLP-based *Update* stage [45, 48] to perform downstream tasks. The critical difference, however, is that cell interactions in NCA evolve over time by recurrent application of the two stages, while ViT computes the token interaction in a single step per layer. During this process, cells dynamically modulate their representations based on the interactions with their neighbors and gradually enlarge their receptive fields. Unlike commonly used convolutional neural networks, NCA maintains resolution during neighborhood expansion, and the parameter sharing across the loop further regularizes the learning process, preventing NCA from overfitting and enhancing its generalization ability [43, 45]. Moreover, NCA

training involves various kinds of stochasticity [44], enabling the models to generalize to input variability and adapt to unpredictable perturbations. It is the modulation of local information and stochasticity during training that make NCA robust against noisy input [48, 47, 54, 61].

However, the original NCA has substantial computational overhead when operating in high-dimensional space, a common scenario in ViTs. This poses a non-trivial challenge when integrating NCA into ViTs. To reduce the dimensionality of interaction results and thus lower the computational cost, we propose *Dynamic Interaction* to replace the standard *Interaction* stage. In addition, tokens dynamically modify the interaction strategy based on the observation of their environment. This adaptation to the variability of the environment contributes to the model robustness. Our modified **Adaptor NCA** (AdaNCA), as a plug-in-play module, improves ViTs performances as illustrated in Figure 1. Adding AdaNCA to different ViT architectures consistently improves their robustness to both adversarial attacks and OOD input. AdaNCA also improves clean accuracy.

Motivated by empirical observations of the positive relationship between network redundancy and model robustness [27], we develop a dynamic programming algorithm to compute the most effective insert position for AdaNCA within a ViT, based on our proposed quantification of network redundancy. Our method results in consistent improvements across 8 robustness benchmarks and 4 different baseline ViT architectures. Critically, we demonstrate that the improvements do not originate from the increase in parameters and FLOPs, but are attributed to AdaNCA. Our contributions are as follows:

- We propose AdaNCA, which integrates Neural Cellular Automata into ViTs’ middle layers as lightweight **Adaptors** to enhance the robustness of ViTs against adversarial attacks and OOD inputs in image classification. With less than 3% more parameters, AdaNCA-extended ViTs can achieve 10% higher accuracy under certain adversarial attacks.
- We introduce *Dynamic Interaction* to replace the *Interaction* stage in standard NCA, enhancing model robustness and efficiency in terms of parameters and computation.
- We propose a method to determine the most effective insert positions of AdaNCA for maximum robustness improvement.

## 2 Related Works

### 2.1 Local structure in Vision Transformer

Since the proposal of Vision Transformer (ViT) [14], a series of works have introduced local structures into ViTs to enhance their performance [8, 10, 16, 21, 22, 36, 41, 51, 67, 69, 70, 72, 74, 75]. Here, we mention one of the earliest local structure modifications and the ones relevant to our work. Stand Alone Self Attention (SASA), as introduced by Ramachandran et al. [53], utilizes sliding window self-attention in ViTs. Following this, Liu et al. [37] develop a non-sliding window attention mechanism that partitions feature maps and computes self-attention both within and between these partitions, termed Shifted Window (Swin) attention. Another method to model local information is convolution. d’Ascoli et al. [16] introduce soft local inductive bias using gated positional self-attention, fusing self-attention and convolution. Despite these advancements in better modeling of local information, few methods contribute to a more robust ViT architecture [41], leaving the models to behave subpar when encountering slightly noisy inputs or distribution shifts.

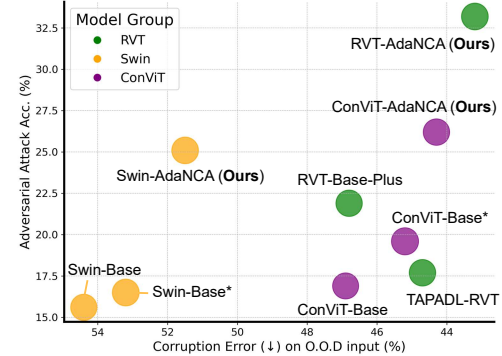


Figure 1: The accuracy under adversarial attacks (APGD-DLR [9]) v.s. corruption error on out-of-distribution input (ImageNet-C [27]) of various ViT models [16, 22, 37, 41]. AdaNCA improves the robustness of different ViTs against both adversarial attacks and OOD input. \*: the same model architecture but with more layers.

2

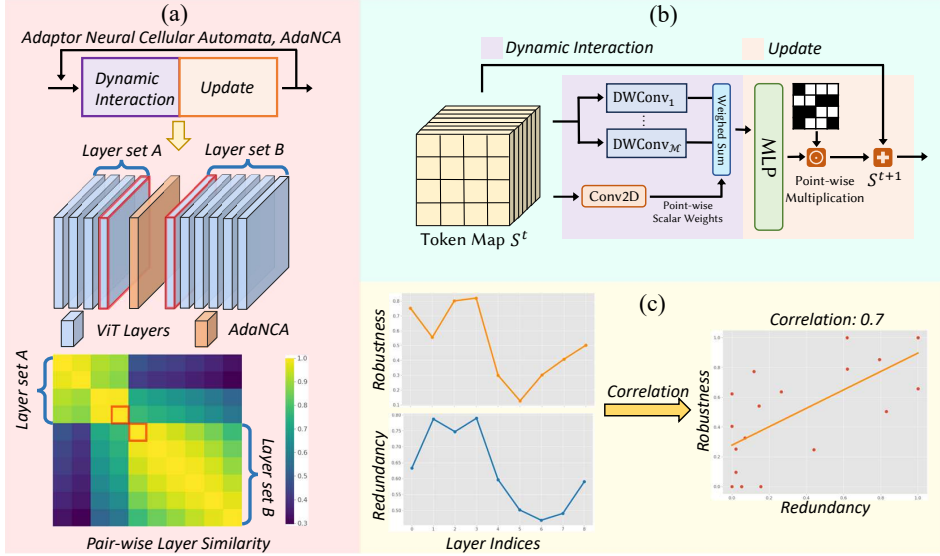


Figure 2: Method overview. (a) Neural Cellular Automata (NCA) can be inserted into Vision Transformers (ViTs) as **Adaptors** to improve model performance and robustness, hence termed AdaNCA. The improvement is maximized when AdaNCA is inserted between two layer sets that each consists of similar layers. (b) A single step of AdaNCA. Our proposed *Dynamic Interaction* contributes to model efficiency as well as robustness. (c) The robustness improvement brought by AdaNCA is highly correlated with the corresponding network redundancy quantification of the insert position. It supports that AdaNCA should be placed between two sets of redundant layers.

## 2.2 Robust architecture in Vision Transformer

Researchers have developed various architectural changes to build more robust ViTs against adversarial attacks, such as FGSM [60] or PGD [40], as well as out-of-distribution (OOD) inputs, such as image corruption [27]. Zhou et al. [77] propose Full Attention Networks to boost the robustness of ViTs against OOD images. Mao et al. [41] first systematically analyze the relationship between different components in a ViT, drawing a positive relationship between convolutional patch embedding as well as convolution in MLP and the robustness of ViTs against adversarial samples and OOD data. Extending [41] and [77], Guo et al. [22] propose input-dependent average pooling to adaptively select different aggregation neighborhoods for different tokens, achieving the state-of-the-art robust ViTs in OOD generalization. Different interpretations of the self-attention operation can also lead to more robust architectures [23, 57]. However, those methods that introduce additional architectures [22, 23, 57, 77] are either implemented on ViTs with limited size or focus on non-adversarial robustness. On the contrary, our method introduces NCA as lightweight plug-in-play adaptors into base-level ViTs, enhancing their clean accuracy and robustness against both adversarial samples and OOD inputs.

## 2.3 Neural Cellular Automata

Mordvintsev et al. [43] propose NCA to mimic the biological cell interactions and model morphogenesis. Following this, several works have applied NCA in computer vision, including texture synthesis [42, 45, 48, 47, 49], image generation [32, 46, 50, 61], and image segmentation [31, 56]. Randazzo et al. [54] propose applying NCA for modeling collective intelligence on image classification tasks, although the limitation to binary images restricts its practical application. Tesfaldet et al. [61] first establish the connection between ViT and NCA via recurrent local attention. However, their application is limited to image inpainting on small datasets such as MNIST [1] and CIFAR10 [35]. Our work first applies NCA in image classification on ImageNet1K with base-level ViT models. Moreover, we propose the new *Dynamic Interaction* for efficient cell interaction modeling, reducing the computational overhead and enhancing the model performance.

### 3 Method

The overview of our method is shown in Figure 2. In this section, we first review the NCA model and ViT architecture in Section 3.1 and establish the connection between NCA and ViT in terms of token interaction modeling. We then present the design of our AdaNCA in Section 3.2. We insert AdaNCA into the middle layers of ViT to improve its robustness, and we introduce the relationship between the insert position of AdaNCA and the relative improvements of model robustness in Section 3.3, which leads to the algorithm for deciding the most effective placement for AdaNCA.

#### 3.1 Preliminaries

**Vision Transformer** Vision Transformers (ViTs) operate on token maps  $\mathbf{X} \in \mathbb{R}^{N \times C}$ , where the number of tokens is  $N$  and each token is represented by a  $C$ -dimensional vector. ViTs learn the interaction between these tokens via self-attention [63] and computes the interaction result  $\mathbf{X}_{attn}$ , as described in Equation 1<sup>1</sup>.

$$\mathbf{X}_{attn} = \sigma \left( \frac{\mathbf{Q}\mathbf{K}^\top}{\sqrt{D}} \right) \mathbf{V}. \quad (1)$$

$\mathbf{Q}$ ,  $\mathbf{K}$ ,  $\mathbf{V}$  stand for query, key, and value, respectively. They are deduced from different linear projections of the input, i.e.,  $\mathbf{Q} = \mathbf{X}\mathbf{W}_Q$ ,  $\mathbf{K} = \mathbf{X}\mathbf{W}_K$ ,  $\mathbf{V} = \mathbf{X}\mathbf{W}_V$ , where  $\mathbf{W}_Q, \mathbf{W}_K, \mathbf{W}_V \in \mathbb{R}^{C \times D}$ .  $D$  is the hidden dimensionality in self-attention.  $\sigma$  is Softmax. After self-attention, tokens are fed into a Multilayer Perceptron (MLP) to get the updated representations  $\mathbf{X}_{out}$ :

$$\mathbf{X}_{out} = f_\theta(\mathbf{X}_{attn}). \quad (2)$$

$f$  is the MLP and  $\theta$  stands for its parameters. The self-attention and MLP form a single ViT block, and one can build a ViT model via stacking ViT blocks.

**Neural Cellular Automata** NCA aims at modeling cell interactions. In the 2D domain, cells live on a 2D grid with size  $H \times W$ . Each cell is represented by a vector with dimensionality  $C$ . All cells collectively define the cell states  $\mathbf{S} \in \mathbb{R}^{H \times W \times C}$ . In a single step of NCA, cells first interact with their neighborhoods for information exchange in the *Interaction* stage [48] to generate the interaction output  $\mathbf{S}_{\mathcal{I}}$ , typically instantiated via depth-wise convolutions [43, 45, 47]:

$$\mathbf{S}_{\mathcal{I}} = (\mathbf{S} \circledast [\mathcal{C}_1, \mathcal{C}_2, \dots, \mathcal{C}_{\mathcal{M}}])_{\oplus}. \quad (3)$$

$\mathcal{C}_i$  is the  $i$ th convolutional kernel, and  $\mathcal{M}$  denotes the total number of kernels. The kernels can either be fixed [48, 47] or learnable [43, 45]. The results of all kernels are concatenated channel-wise in the  $\oplus$  operation.  $\mathbf{S}_{\mathcal{I}}$  is then passed to an MLP in the *Update* stage [48], where cells get the updated states  $\mathbf{S}_{out}$ :

$$\mathbf{S}_{out} = f_\theta(\mathbf{S}_{\mathcal{I}}) \odot \mathbf{M}. \quad (4)$$

$f$  is the MLP and  $\theta$  stands for its parameters. Typically, NCA uses the simplest MLP with two linear layers and one activation between them.  $\mathbf{M} \in \mathbb{R}^{H \times W \times C}$ , sampled from  $Bernoulli(p)$ , is a random binary mask to introduce stochasticity in NCA, ensuring asynchronicity during the cell updates [44].  $\odot$  is point-wise multiplication. NCA learns an underlying dynamic governing the cell behaviors [49], as depicted by the stochastic differential equation (SDE) in Equation 5:

$$\frac{\partial \mathbf{S}}{\partial t} = \mathcal{F}_\Theta(\mathbf{S}) \odot \mathbf{M} = f_\theta([\mathbf{S} \circledast [\mathcal{C}_1, \mathcal{C}_2, \dots, \mathcal{C}_{\mathcal{M}}]]_{\oplus}) \odot \mathbf{M}. \quad (5)$$

$\mathcal{F}$  represents operations in *Interaction* as well as *Update* stages.  $\Theta$  is the set containing trainable parameters in the two stages. Discretizing the SDE with  $\Delta t = 1$  naturally results in a recurrent residual update scheme:

$$\mathbf{S}^{t+1} = \mathbf{S}^t + \mathcal{F}_\Theta(\mathbf{S}^t) \odot \mathbf{M}. \quad (6)$$

NCA outputs the cell states at time  $t = T$  to accomplish downstream tasks.  $T$  is a randomly-chosen integer in a certain range.

<sup>1</sup>We ignore the residual update scheme for simplicity

### 3.1.1 Connecting NCA and ViT

Both NCA and ViT learn interactions between a set of elements, i.e., tokens in ViT and cells in NCA. From now on, we refer to a cell in NCA as a token, aligning it with the concept in ViTs. The asynchronicity [44] introduced by the random mask  $M$  can be regarded as a cell-wise stochastic depth [30], a more fine-grained version of the sample-wise stochastic depth. In previous NCA works, stochasticity is maintained during testing [45]. Such a scheme is problematic in discriminative tasks since reliable numerical outputs are essential. To this end, we adopt the strategy in dropout-like techniques [58, 30] that compensates activation values during training. Given  $M \sim Bernoulli(p)$ , the evolution of NCA in AdaNCA is defined as:

$$\text{Train} : \mathbf{S}^{t+1} = \mathbf{S}^t + \frac{\mathcal{F}_\Theta(\mathbf{S}^t)}{p} \odot M; \quad \text{Test} : \mathbf{S}^{t+1} = \mathbf{S}^t + \mathcal{F}_\Theta(\mathbf{S}^t). \quad (7)$$

Furthermore, NCA typically queries the cell states at a random time step  $T$ , resulting in random update steps for all cells. Such randomness ensures the stability of NCA across various time steps [43]. Hence, the trained model can effectively handle the variability and unpredictability of the input, thus being robust against noisy input. Our ablation studies in Section 4.3 demonstrate the effectiveness of these two strategies in enhancing the model performance and robustness.

## 3.2 AdaNCA architecture

The architecture of AdaNCA is shown in Figure 3. It shares a similar update scheme with the standard NCA as described in Equation 7, but is more computationally efficient due to the proposed *Dynamic Interaction* stage. All convolutional kernels for token interaction are trainable. In the following paragraphs, we first present the design of the *Dynamic Interaction* stage and then introduce a way for more efficient token interaction using multi-scale *Dynamic Interaction*.

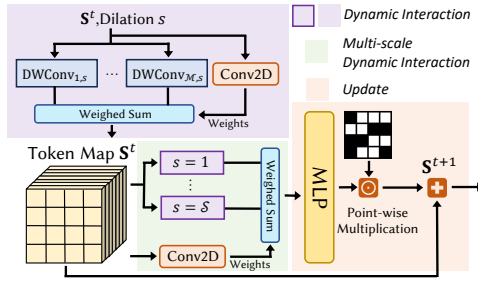


Figure 3: Overview of AdaNCA architecture.

### 3.2.1 Dynamic Interaction

The *Interaction* stage in the original NCA performs channel-wise concatenation of the results from different depth-wise convolutions. Instead, our *Dynamic Interaction* computes a weighted sum of those results. Specifically, a weight computation module  $\mathcal{W}_I$  takes the token map as input and outputs per-token scalar weights  $\mathbf{W}_{Im} \in \mathbb{R}^{H \times W \times 1}$ . We modify Equation 3 to Equation 8:

$$\mathbf{S}_{DI} = \sum (\mathbf{S} * \mathcal{W}_I)(\mathbf{S} \circledast [\mathcal{C}_1, \mathcal{C}_2, \dots, \mathcal{C}_M]) = \sum (\mathbf{S} * \mathcal{W}_I)\mathbf{S}_m = \sum_{m=1}^M \sum_{c=1}^C \mathbf{W}_{Im} \odot \mathbf{S}_{mc}, \quad (8)$$

where  $\mathbf{S}_{mc} \in \mathbb{R}^{H \times W \times 1}$ ,  $\mathbf{S}_{DI} \in \mathbb{R}^{H \times W \times C}$ . We instantiate the weight computation module  $\mathcal{W}_I$  using a two-layer convolutional network. The first layer transforms the dimensionality from  $C$  to  $M$ , and the second layer computes the actual weights, producing  $M$  scalars for each token. Both layers use  $3 \times 3$  convolutions to factor in information from both the token and its neighbors. To stabilize training, we add a batch normalization between the two convolutions. Our design of the weight computation network coincides with the one in [22], although our focus is on extracting various information from the same neighborhoods rather than aggregating data from different neighborhoods.

### 3.2.2 Multi-scale Dynamic Interaction

Inspired by [47] that uses multi-scale token *Interaction* to facilitate long-range token communication, we propose multi-scale *Dynamic Interaction*. Concretely, all convolutions in Equation 8 now have one more degree of freedom in dilation. Dilation  $s$  represents the current operating scale being  $s$ , and  $s \in \{1, 2, \dots, S\}$ . Hence, the original *Dynamic Interaction* is a special case where  $S = 1$ . To

increase the feature expressivity, we perform a weighted sum on the outputs of all scales, where the per-token weights  $\mathbf{W}_{Ms}$  are generated by a network  $\mathcal{W}_M$  as described in Equation 9.

$$\mathbf{S}_{MDI} = \sum (\mathbf{S} * \mathcal{W}_M) \mathbf{S}_{DI} = \sum (\mathbf{S} * \mathcal{W}_M) \mathbf{S}_{DI} = \sum_{s=1}^S \sum_{c=1}^C \mathbf{W}_{Ms} \odot \mathbf{S}_{DIsc}, \quad (9)$$

where  $\mathbf{W}_{Ms}, \mathbf{S}_{DIsc} \in \mathbb{R}^{H \times W \times 1}$ ,  $\mathbf{S}_{MDI}, \mathbf{S}_{DI} \in \mathbb{R}^{H \times W \times C}$ . The weight computation network  $\mathcal{W}_M$  shares the same structure with  $\mathcal{W}_I$  in the *Dynamic Interaction*.

### 3.3 Insert positions of AdaNCA

Given a ViT and an AdaNCA, we need to determine where to insert AdaNCA to maximize the robustness improvements. To this end, we first establish the correlation between the placement of AdaNCA and the robustness enhancement it brings. Motivated by the fact that the network redundancy contributes to the model robustness [27], we hypothesize that the effect of AdaNCA should correlate to the layer redundancy corresponding to the insert position. To quantify the redundancy, we propose the **Set Cohesion Index**  $\kappa$ . Given a trained model with  $L$  layers and two layer indices  $i, j \in \{1, 2, \dots, L\}$  where  $i < j$ ,  $\kappa(i, j)$  is defined in Equation 10.

$$\begin{aligned} \kappa(i, j) = & \frac{1}{(j - i + 1)^2} \sum_{m, n \in [i, j]} \text{Sim}(m, n) - \frac{\mathbb{1}_{i > 1}}{(i - 1)(j - i + 1)} \sum_{m_1 \in [1, i - 1], n \in [i, j]} \text{Sim}(m_1, n) \\ & - \frac{\mathbb{1}_{j < L}}{(L - j)(j - i + 1)} \sum_{m \in [i, j], n_1 \in [j + 1, L]} \text{Sim}(m, n_1) \end{aligned} \quad (10)$$

$\mathbb{1}$  stands for the indicator function.  $\text{Sim}(m, n)$  is the function for quantifying the output similarity between layer  $m$  and  $n$ . We choose Centered Kernel Alignment (CKA) [34], a common metric for measuring layer similarities inside or between neural networks [24]. A higher  $\kappa$  stands for a more cohesive layer set defined by layers from  $i$  to  $j$ . Inserting AdaNCA after layer  $i$  would partition the network into 2 layer sets, and we can compute the sum of  $\kappa$  of the layers before and after  $i$ , i.e.  $\mathcal{K}(i) = \kappa(1, i) + \kappa(i + 1, L)$ , serving as a quantification of the network redundancy corresponding to position  $i$ . We assume that AdaNCA will not change the layer similarity structure since it is too small compared to a single layer in all ViTs.

On the other hand, we quantify the robustness improvement brought by AdaNCA using the relative increase in the attack failure rate of the AdaNCA-inserted models and the corresponding baseline. Specifically, if a model can achieve  $\alpha$  clean test accuracy as well as  $\alpha'$  accuracy under adversarial attacks, the attack failure rate is  $\beta = \frac{\alpha'}{\alpha}$ . The robustness improvement  $\gamma$  is then defined as  $\gamma = \frac{\beta_{AdaNCA} - \beta_{base}}{\beta_{base}}$ . In our experiments, we find that  $\gamma$  is significantly correlated with the network redundancy  $\mathcal{K}$  ( $r = 0.6938, p < 0.001$ ). We refer readers to Appendix A for details of the experiments. The results validate our hypothesis and indicate that AdaNCA should be inserted into the position that can maximize network redundancy. We develop a dynamic programming algorithm to find those positions and refer readers to Appendix A.1 for the details.

## 4 Experiments

We choose 4 ViT models as the baseline: Swin-base (Swin-B) [37], FAN-Base-Hybrid (FAN-B) [77], RVT-Base-Plus (RVT-B) [41], and ConViT-Base (ConViT-B) [16]. Our choices include a hierarchical model (Swin), a convolution-attention hybrid model (FAN), and two regular models in which all layers share the same structure (RVT and ConViT). RVT is specifically built to be a robust model while ConViT is not. All 4 models are already equipped with different kinds of local structures. Moreover, we choose two SOTA models in terms of robustness against out-of-distribution (OOD) data, TAPADL-RVT and TAPADL-FAN [22] for comparison. Note that the SOTA method involves training with an additional loss (ADL) while we do not incorporate it in our training, since our focus is on the effect of architectural changes. We follow the training scheme for each model, respectively, to train the AdaNCA-equipped model from scratch on ImageNet1K. We conduct the analysis presented in Section 3.3 to decide the optimal position to insert multiple AdaNCA modules, in which the ImageNet1K pre-trained weights for analysis are obtained from the PyTorch Image Models library [68]. To balance between the computational cost and robustness improvement, we limit the number of AdaNCA to 2 or 3, depending on the model architecture. The recurrent time step of all AdaNCA

Table 1: The performance of AdaNCA-enhanced ViTs and their corresponding baselines. AdaNCA consistently improves the clean accuracy as well as the robustness to adversarial and out-of-distribution inputs of the baseline models. Note that our models also outperform the larger baselines (\* sign), indicating that the performance improvement does not merely originate from the increase in the number of parameters or FLOPs. The TAPADL method [22] can lead to more vulnerable models compared to the baselines (green numbers).  $\dagger$ : the test is conducted on models pre-trained on ImageNet22K [41], see Appendix C.8.

Model	Params (M)	FLOPs (G)	ImageNet Clean Acc.	Adversarial Inputs					OOD inputs		
				PGD	CW	APGD-DLR	APGD-CE	IM-A	IM-C (↓)	IM-R	IM-SK
RVT-B [41]	88.5	17.7	82.7	29.9	21.5 $\dagger$	21.9 $\dagger$	31.4 $\dagger$	28.5	46.8	48.7	36.0
TAPADL-RVT [22]	89.4	17.9	83.1	27.6	19.3	17.7	26.8	32.5	44.7	50.2	38.6
<b>RVT-B-AdaNCA</b>	<b>91.0</b>	<b>19.0</b>	<b>83.3</b>	<b>36.7</b>	<b>30.2</b>	<b>33.2</b>	<b>36.2</b>	<b>31.9</b>	<b>43.2</b>	<b>51.7</b>	<b>39.0</b>
FAN-B [77]	50.4	11.7	83.9	15.0	7.6	10.4	13.1	39.6	46.1	52.7	40.8
TAPADL-FAN [22]	50.7	11.8	<b>84.3</b>	18.6	9.2	13.5	16.9	41.8	<b>43.7</b>	52.9	<b>40.7</b>
<b>FAN-B-AdaNCA</b>	<b>51.7</b>	<b>12.4</b>	<b>84.1</b>	<b>20.3</b>	<b>10.6</b>	<b>14.1</b>	<b>19.1</b>	<b>42.9</b>	44.7	<b>53.4</b>	<b>41.0</b>
Swin-B [37]	87.8	15.4	83.4	21.3	13.4	15.6	23.1	35.8	54.3	46.6	32.4
Swin-B* [37]	94.1	16.7	83.3	22.8	14.6	15.9	23.8	35.2	53.2	46.9	33.7
<b>Swin-B-AdaNCA</b>	<b>90.7</b>	<b>16.3</b>	<b>83.7</b>	<b>24.1</b>	<b>20.5</b>	<b>25.1</b>	<b>24.8</b>	<b>36.0</b>	<b>51.5</b>	<b>48.2</b>	<b>35.5</b>
ConViT-B [16]	86.5	17.7	82.4	21.2	8.9	16.9	20.3	29.0	46.9	48.4	35.7
ConViT-B* [16]	93.6	19.2	82.7	24.1	10.0	20.5	23.9	30.1	45.2	49.9	37.8
<b>ConViT-B-AdaNCA</b>	<b>89.0</b>	<b>19.0</b>	<b>83.2</b>	<b>29.2</b>	<b>20.1</b>	<b>26.3</b>	<b>28.4</b>	<b>33.0</b>	<b>44.3</b>	<b>51.1</b>	<b>39.1</b>

Table 2: Comparisons of corruption error on each corruption type of ImageNet-C. AdaNCA consistently improves the performance of the baseline model in all categories (Swin-B), and can achieve better results in most categories compared to the SOTA method (TAPADL-RVT).

Model	mCE	Noise			Blur				Weather			Digital				
		Gauss	Shot	Impulse	Defocus	Glass	Motion	Zoom	Snow	Frost	Fog	Bright	Contrast	Elastic	Pixelate	JPEG
Swin-B [37]	54.3	43.8	45.7	43.8	61.6	73.2	55.5	66.5	50.0	47.4	47.9	42.1	38.7	68.8	66.4	62.6
<b>Swin-B-AdaNCA</b>	<b>51.5</b>	<b>39.5</b>	<b>40.9</b>	<b>39.8</b>	<b>59.5</b>	<b>69.5</b>	<b>55.0</b>	<b>65.6</b>	<b>49.4</b>	<b>47.1</b>	<b>40.8</b>	<b>40.6</b>	<b>37.0</b>	<b>66.3</b>	<b>59.9</b>	<b>61.1</b>
TAPADL-RVT [22]	44.7	34.6	36.1	34.0	53.9	62.3	52.2	<b>60.1</b>	<b>41.9</b>	44.9	35.8	37.4	31.9	57.1	41.1	47.2
<b>RVT-B-AdaNCA</b>	<b>43.2</b>	<b>33.9</b>	<b>36.1</b>	<b>33.9</b>	<b>52.7</b>	<b>59.1</b>	<b>47.8</b>	60.5	42.6	<b>39.0</b>	<b>33.9</b>	<b>36.8</b>	<b>31.7</b>	<b>53.4</b>	<b>40.0</b>	<b>46.2</b>

is chosen from  $\{[2, 2], [2, 4], [3, 5]\}$ , and we follow the design principle of ViT, which is to put more computation in the middle or high layers [37]. **We fix the random steps during test to a single integer chosen from the range** to get precise results and ensure non-stochasticity during adversarial attacks. All the activation functions used in the MLP in AdaNCA are GELU [28], and the input, hidden, and output dimensionalities of the MLP are all the same. We refer readers to Appendix C.6 for the details of the training and insert scheme of AdaNCA. All of our experiments are performed on 4 Nvidia A100 GPUs.

#### 4.1 Results on Image Classification

We test all models on the ImageNet1K validation set for clean accuracy. For the adversarial robustness evaluation, we choose common adversarial attack methods PGD [40], CW [5], APGD-DLR [9], and APGD-CE [9]. Moreover, we also include the natural adversarial examples in ImageNet-A (IM-A) [13]. For the PGD attack, we align with the settings used in [41]: max magnitude  $\epsilon = 1$ , step size  $\alpha = 0.5$ , steps  $t = 5$ . We refer readers to the Appendix C.7 for details of the other attacks. For testing the OOD generalization, we use ImageNet-C (IM-C) [27], ImageNet-R (IM-R) [29], and ImageNet-Sketch (IM-SK) [66]. We report the mean corruption error (mCE) on ImageNet-C and accuracy on all other kinds of robustness benchmarks in Table 1. Our results highlight that AdaNCA-enhanced ViTs consistently outperform corresponding baselines in various robustness tests as well as in terms of clean accuracy. Importantly, the enlarged baseline models (\* sign) do not bring comparable improvements to AdaNCA, suggesting that the enhancements do not merely stem from the increase in computational budgets. However, the existing method [22] that introduces local structure into ViTs can potentially undermine the adversarial robustness of the baselines. In Table 2, we conduct an in-depth study on the corruption errors of the different categories of common corruptions in ImageNet-C. The results show that AdaNCA enhances robustness without the trade-off seen in methods that ignore texture information [17, 52]. While these methods may improve mCE for non-Blur noise, they often worsen mCE for Blur noise [52]. In contrast, AdaNCA consistently improves robustness across most categories. We refer readers to Appendix C for more results.

#### 4.2 Layer similarity structure

Our key assumption in Section 3.3 is that AdaNCA will not change the layer similarity structure due to its small size, and that is why we use **pre-trained** networks to conduct the analysis. Here, we

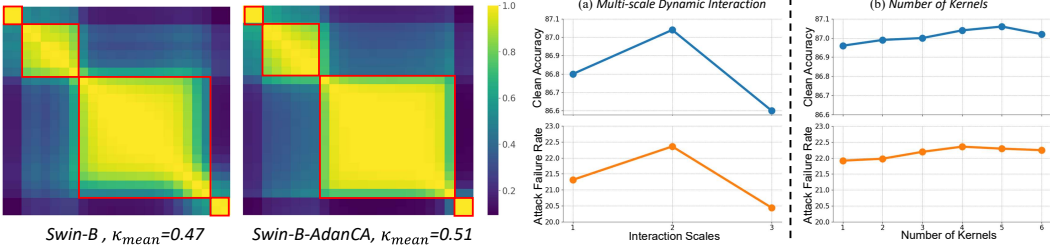


Figure 4: Pair-wise layer similarities. Layer sets are marked in **red boxes**. Swin-B-AdanCA has a clearer stage partition.

Figure 5: Ablation on the (a) scales and (b) number of kernels used in our multi-scale *Dynamic Interaction*. We choose  $\mathcal{S} = 2$ ,  $\mathcal{M} = 4$  to balance between the **clean accuracy** and **robustness**.

examine the pair-wise layer similarities in Swin-B [37] and Swin-B-AdaNCA in Figure 4.  $\kappa_{mean}$  is the mean of  $\kappa$  from all layer sets. We refer readers to Appendix C.11 for more results. AdaNCA not only preserves the original layer similarity structure but also contributes to a clearer stage partition, validating our assumption in Section 3.3. The results might be attributed to the fact that AdaNCA transmits information between different layer sets and thus layers inside each set do not bother adapting to the layers outside the set.

### 4.3 Ablation studies

We conduct ablation studies on ImageNet100, a 100-class subset of ImageNet1K. Previous studies [7, 15, 71, 73] have shown that ImageNet100 serves as a representative subset of ImageNet1K. Hence, we can obtain representative results for the self-evaluation of the model while efficiently using the computational resources. All the ablation experiments are based on a Swin-tiny [37] model. We insert it after the fourth layer to obtain the best robustness improvement, according to our analysis in Section 3.3 and Appendix A. First, we ablate on two hyperparameters, the number of convolutional kernels used in the *Dynamic Interaction* stage ( $\mathcal{M}$ ) and the maximum scale ( $\mathcal{S}$ ) used in the multi-scale *Dynamic Interaction* stage. The **Clean Accuracy** and **Attack Failure Rate** are shown in Figure 5. The attack failure rate is quantified using the same method as in Section 3.3 and Appendix A. Multi-scale interaction can contribute to the performance while overly large scale can lose local information. Increasing the number of kernels benefits the performance while too many kernels undermine the robustness. According to the results, we choose  $\mathcal{S} = 2$ ,  $\mathcal{M} = 4$ . We then perform ablations on several design choices:

- **Recurrent update (Recur).** Ablation on unrolling the recurrence with average time step  $T$  in AdaNCA into  $T$  independent AdaNCA with time step being 1.
- **Stochastic update (StocU).** Ablate the stochastic update during training, leading to globally synchronized update of all tokens [44].
- **Random step (RandS).** Change the recurrence time step from a randomly chosen integer in range  $[T_1, T_2]$  to  $\lceil (T_1 + T_2)/2 \rceil$ . It cannot be turned on without recurrence.
- **Dynamic interaction (DynIn).** Ablate the *Dynamic Interaction* that the interaction results are simply summed together. The number of kernels remains the same.

Results are shown in Table 3. Our design choices contribute to model performance and robustness.

### 4.4 Noise sensitivity examination

A drawback of adversarially robust models is their increased sensitivity to noise in specific frequency bands [59]. For instance, while adversarially trained models are robust against adversarial attacks, they can be sensitive to noise from a larger frequency-band range compared to standard models [59]. Here, we use the method and data from [59] to examine the noise sensitivity of AdaNCA-enhanced ViTs. Specifically, we evaluate the classification performance on a set of images that are mixed with noise of varying magnitudes and frequencies.

Table 3: Ablation studies on design choices. Each of the AdaNCA design choices contributes to improved performance and robustness. Baseline is a Swin-tiny [37] model trained on ImageNet-100.

Exp. Type	Recur	StocU	RandS	DynIn	Params (M)	FLOPs (G)	Accuracy	Attack Failure Rate
Baseline	<b>X</b>	<b>X</b>	<b>X</b>	<b>X</b>	27.69	4.5	86.56	12.29
Ablation	<b>X</b>	<b>✓</b>	<b>X</b>	<b>✓</b>	28.97	4.7	<b>87.36</b>	19.04
	<b>✓</b>	<b>X</b>	<b>✓</b>	<b>✓</b>	27.94	4.7	86.92	19.56
	<b>✓</b>	<b>✓</b>	<b>X</b>	<b>✓</b>	27.94	4.7	87.12	19.34
	<b>✓</b>	<b>✓</b>	<b>✓</b>	<b>X</b>	27.93	4.7	86.72	21.98
<b>Ours</b>	<b>✓</b>	<b>✓</b>	<b>✓</b>	<b>✓</b>	27.94	4.7	87.18	<b>22.35</b>

Higher classification accuracy on a specific noise type indicates that the model is less sensitive to that noise. Figure 6 presents the results, including human data sourced from [59]. Our findings demonstrate that AdaNCA enhances ViTs by reducing the sensitivity to noise with certain frequency components, equipping ViTs with more human-like noise-resilient abilities. Crucially, AdaNCA improves the model robustness differently than adversarial training since the AdaNCA-enhanced ViTs do not exhibit increased sensitivity to the noise. We quantitatively validate the conclusion and refer readers to Appendix C.13 for the details.

## 5 Limitation

AdaNCA has certain limitations. First, the AdaNCA-equipped ViTs cannot adapt to unseen recurrent steps of AdaNCA, limiting the generalization ability. For example, if the training step range of AdaNCA is [3,5], it cannot produce meaningful results with the test step being 6. Moreover, AdaNCA introduces non-neglectable computation into the original architecture. Furthermore, our experiments are conducted on ImageNet1K with the image size being  $224 \times 224$ . Whether AdaNCA can lead to impressive improvement on larger-scale problems, *e.g.*, ImageNet22K, remains a question. The size of the images can also affect the efficiency of token interaction.

## 6 Broader Impact

AdaNCA contributes to more robust ViTs, facilitating their usage in real-world scenarios. Moreover, we bridge two powerful models, NCA and ViT, on large-scale image classification, potentially encouraging research dedicated to their synergistic combination in more practical settings. Our finding on AdaNCA improving network redundancy can stimulate more works on architectural robustness in deep learning, which involves increasing the redundancy to enhance robustness.

## 7 Conclusion

We propose AdaNCA, an efficient Neural Cellular Automata (NCA) that, when inserted between their middle layers, improves ViT performances and robustness against adversarial attacks as well as out-of-distribution inputs. We motivate our design by connecting NCA and ViT in terms of token interaction modeling, and propose *Dynamic Interaction* to improve the computational efficiency of standard NCA. Exploiting the training strategies and design choices in NCA, *i.e.*, stochastic update, random steps, and multi-scale interaction, we further enhance the AdaNCA-enhanced ViTs’ clean accuracy and robustness. To decide the placement of AdaNCA, we propose the Set Cohesion Index that quantifies the network redundancy via layer similarity and conclude that AdaNCA should be inserted between two layer sets that consist of redundant layers. Our results demonstrate that AdaNCA consistently improves ViTs performances and robustness. Evidence suggests that the mechanism by which we obtain improvement reduces the sensitivity of ViTs to certain types of noise and makes the noise-resilient ability of ViTs closer to humans.

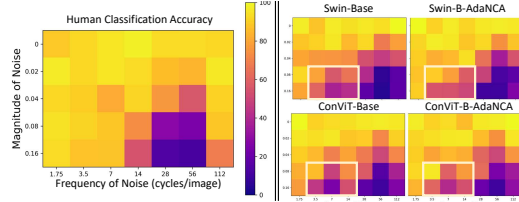


Figure 6: Classification accuracy of humans and ViTs on noisy images. AdaNCA improves the accuracy on images with certain types of noise (yellow boxes), indicating that it makes ViTs less sensitive to them. Quantitative: Appendix C.13.

## References

- [1] The MNIST database of handwritten digits. <http://yann.lecun.com/exdb/mnist/>.
- [2] Maksym Andriushchenko, Francesco Croce, Nicolas Flammarion, and Matthias Hein. Square attack: a query-efficient black-box adversarial attack via random search. In *European Conference on Computer Vision*, pages 484–501. Springer, 2020.
- [3] Anish Athalye, Nicholas Carlini, and David Wagner. Obfuscated gradients give a false sense of security: Circumventing defenses to adversarial examples. In *International Conference on Machine Learning*, pages 274–283. PMLR, 2018.
- [4] Srinadh Bhojanapalli, Ayan Chakrabarti, Daniel Glasner, Daliang Li, Thomas Unterthiner, and Andreas Veit. Understanding robustness of transformers for image classification. In *Proceedings of the IEEE/CVF international conference on computer vision*, pages 10231–10241, 2021.
- [5] Nicholas Carlini and David Wagner. Towards evaluating the robustness of neural networks. In *2017 IEEE Symposium on Security and Privacy (SP)*, pages 39–57. Ieee, 2017.
- [6] Aditya Chattpadhyay, Anirban Sarkar, Prantik Howlader, and Vineeth N Balasubramanian. Grad-cam++: Generalized gradient-based visual explanations for deep convolutional networks. In *2018 IEEE winter conference on applications of computer vision (WACV)*, pages 839–847. IEEE, 2018.
- [7] Yixin Cheng, Grigorios Chrysos, Markos Georgopoulos, and Volkan Cevher. Multilinear operator networks. In *The Twelfth International Conference on Learning Representations*, 2023.
- [8] Xiangxiang Chu, Zhi Tian, Bo Zhang, Xinlong Wang, and Chunhua Shen. Conditional positional encodings for vision transformers. In *The Eleventh International Conference on Learning Representations*, 2022.
- [9] Francesco Croce and Matthias Hein. Reliable evaluation of adversarial robustness with an ensemble of diverse parameter-free attacks. In *International Conference on Machine Learning*, pages 2206–2216. PMLR, 2020.
- [10] Zihang Dai, Hanxiao Liu, Quoc V Le, and Mingxing Tan. Coatnet: Marrying convolution and attention for all data sizes. *Advances in Neural Information Processing Systems*, 34:3965–3977, 2021.
- [11] Mostafa Dehghani, Josip Djolonga, Basil Mustafa, Piotr Padlewski, Jonathan Heek, Justin Gilmer, Andreas Peter Steiner, Mathilde Caron, Robert Geirhos, Ibrahim Alabdulmohsin, et al. Scaling vision transformers to 22 billion parameters. In *International Conference on Machine Learning*, pages 7480–7512. PMLR, 2023.
- [12] Jia Deng, Wei Dong, Richard Socher, Li-Jia Li, Kai Li, and Li Fei-Fei. Imagenet: A large-scale hierarchical image database. In *2009 IEEE Conference on Computer Vision and Pattern Recognition*, pages 248–255. Ieee, 2009.
- [13] Josip Djolonga, Jessica Yung, Michael Tschannen, Rob Romijnders, Lucas Beyer, Alexander Kolesnikov, Joan Puigcerver, Matthias Minderer, Alexander D’Amour, Dan Moldovan, et al. On robustness and transferability of convolutional neural networks. In *Proceedings of the IEEE/CVF Conference on Computer Vision and Pattern Recognition*, pages 16458–16468, 2021.
- [14] Alexey Dosovitskiy, Lucas Beyer, Alexander Kolesnikov, Dirk Weissenborn, Xiaohua Zhai, Thomas Unterthiner, Mostafa Dehghani, Matthias Minderer, Georg Heigold, Sylvain Gelly, et al. An image is worth 16x16 words: Transformers for image recognition at scale. In *International Conference on Learning Representations*, 2020.
- [15] Arthur Douillard, Alexandre Ramé, Guillaume Couairon, and Matthieu Cord. Dytok: Transformers for continual learning with dynamic token expansion. In *Proceedings of the IEEE/CVF Conference on Computer Vision and Pattern Recognition*, pages 9285–9295, 2022.

[16] Stéphane d’Ascoli, Hugo Touvron, Matthew L Leavitt, Ari S Morcos, Giulio Biroli, and Levent Sagun. Convit: Improving vision transformers with soft convolutional inductive biases. In *International Conference on Machine Learning*, pages 2286–2296. PMLR, 2021.

[17] Robert Geirhos, Patricia Rubisch, Claudio Michaelis, Matthias Bethge, Felix A Wichmann, and Wieland Brendel. Imagenet-trained cnns are biased towards texture; increasing shape bias improves accuracy and robustness. In *International Conference on Learning Representations*, 2018.

[18] Robert Geirhos, Jörn-Henrik Jacobsen, Claudio Michaelis, Richard Zemel, Wieland Brendel, Matthias Bethge, and Felix A Wichmann. Shortcut learning in deep neural networks. *Nature Machine Intelligence*, 2(11):665–673, 2020.

[19] Jacob Gildenblat and contributors. Pytorch library for cam methods. <https://github.com/jacobgil/pytorch-grad-cam>, 2021.

[20] Andrey Gromov, Kushal Tirumala, Hassan Shapourian, Paolo Glorioso, and Daniel A Roberts. The unreasonable ineffectiveness of the deeper layers. *arXiv preprint arXiv:2403.17887*, 2024.

[21] Jianyuan Guo, Kai Han, Han Wu, Yehui Tang, Xinghao Chen, Yunhe Wang, and Chang Xu. Cmt: Convolutional neural networks meet vision transformers. In *Proceedings of the IEEE/CVF Conference on Computer Vision and Pattern Recognition*, pages 12175–12185, 2022.

[22] Yong Guo, David Stutz, and Bernt Schiele. Robustifying token attention for vision transformers. In *Proceedings of the IEEE/CVF International Conference on Computer Vision*, pages 17557–17568, 2023.

[23] Xing Han, Tongzheng Ren, Tan Nguyen, Khai Nguyen, Joydeep Ghosh, and Nhat Ho. Designing robust transformers using robust kernel density estimation. *Advances in Neural Information Processing Systems*, 36, 2024.

[24] Yena Han, Tomaso A Poggio, and Brian Cheung. System identification of neural systems: If we got it right, would we know? In *International Conference on Machine Learning*, pages 12430–12444. PMLR, 2023.

[25] Ali Hassani, Steven Walton, Jiachen Li, Shen Li, and Humphrey Shi. Neighborhood attention transformer. In *Proceedings of the IEEE/CVF Conference on Computer Vision and Pattern Recognition*, pages 6185–6194, 2023.

[26] Kaiming He, Xiangyu Zhang, Shaoqing Ren, and Jian Sun. Deep residual learning for image recognition. In *Proceedings of the IEEE conference on computer vision and pattern recognition*, pages 770–778, 2016.

[27] Dan Hendrycks and Thomas Dietterich. Benchmarking neural network robustness to common corruptions and perturbations. In *International Conference on Learning Representations*, 2018.

[28] Dan Hendrycks and Kevin Gimpel. Gaussian error linear units (gelus). *arXiv preprint arXiv:1606.08415*, 2016.

[29] Dan Hendrycks, Steven Basart, Norman Mu, Saurav Kadavath, Frank Wang, Evan Dorundo, Rahul Desai, Tyler Zhu, Samyak Parajuli, Mike Guo, et al. The many faces of robustness: A critical analysis of out-of-distribution generalization. In *Proceedings of the IEEE/CVF International Conference on Computer Vision*, pages 8340–8349, 2021.

[30] Gao Huang, Yu Sun, Zhuang Liu, Daniel Sedra, and Kilian Q Weinberger. Deep networks with stochastic depth. In *Computer Vision–ECCV 2016: 14th European Conference, Amsterdam, The Netherlands, October 11–14, 2016, Proceedings, Part IV 14*, pages 646–661. Springer, 2016.

[31] John Kalkhof, Camila González, and Anirban Mukhopadhyay. Med-nca: Robust and lightweight segmentation with neural cellular automata. In *International Conference on Information Processing in Medical Imaging*, pages 705–716. Springer, 2023.

[32] John Kalkhof, Arlene Kühn, Yannik Frisch, and Anirban Mukhopadhyay. Frequency-time diffusion with neural cellular automata. *arXiv preprint arXiv:2401.06291*, 2024.

[33] Hoki Kim. Torchattacks: A pytorch repository for adversarial attacks. *arXiv preprint arXiv:2010.01950*, 2020.

[34] Simon Kornblith, Mohammad Norouzi, Honglak Lee, and Geoffrey Hinton. Similarity of neural network representations revisited. In *International Conference on Machine Learning*, pages 3519–3529. PMLR, 2019.

[35] Alex Krizhevsky, Geoffrey Hinton, et al. Learning multiple layers of features from tiny images. 2009.

[36] Yawei Li, Kai Zhang, Jiezhang Cao, Radu Timofte, Michele Magno, Luca Benini, and Luc Van Gool. Localvit: Analyzing locality in vision transformers. In *2023 IEEE/RSJ International Conference on Intelligent Robots and Systems (IROS)*, pages 9598–9605. IEEE, 2023.

[37] Ze Liu, Yutong Lin, Yue Cao, Han Hu, Yixuan Wei, Zheng Zhang, Stephen Lin, and Baining Guo. Swin transformer: Hierarchical vision transformer using shifted windows. In *Proceedings of the IEEE/CVF International Conference on Computer Vision*, pages 10012–10022, 2021.

[38] Ze Liu, Han Hu, Yutong Lin, Zhuliang Yao, Zhenda Xie, Yixuan Wei, Jia Ning, Yue Cao, Zheng Zhang, Li Dong, et al. Swin transformer v2: Scaling up capacity and resolution. In *Proceedings of the IEEE/CVF Conference on Computer Vision and Pattern Recognition*, pages 12009–12019, 2022.

[39] Zhuang Liu, Hanzi Mao, Chao-Yuan Wu, Christoph Feichtenhofer, Trevor Darrell, and Saining Xie. A convnet for the 2020s. In *Proceedings of the IEEE/CVF Conference on Computer Vision and Pattern Recognition*, pages 11976–11986, 2022.

[40] Aleksander Madry, Aleksandar Makelov, Ludwig Schmidt, Dimitris Tsipras, and Adrian Vladu. Towards deep learning models resistant to adversarial attacks. In *International Conference on Learning Representations*, 2018.

[41] Xiaofeng Mao, Gege Qi, Yuefeng Chen, Xiaodan Li, Ranjie Duan, Shaokai Ye, Yuan He, and Hui Xue. Towards robust vision transformer. In *Proceedings of the IEEE/CVF Conference on Computer Vision and Pattern Recognition*, pages 12042–12051, 2022.

[42] Alexander Mordvintsev and Eyvind Niklasson.  $\mu$ nca: Texture generation with ultra-compact neural cellular automata. *arXiv preprint arXiv:2111.13545*, 2021.

[43] Alexander Mordvintsev, Ettore Randazzo, Eyvind Niklasson, and Michael Levin. Growing neural cellular automata. *Distill*, 2020. doi: 10.23915/distill.00023. <https://distill.pub/2020/growing-ca>.

[44] Eyvind Niklasson, Alexander Mordvintsev, and Ettore Randazzo. Asynchronicity in neural cellular automata. In *Artificial Life Conference Proceedings 33*, volume 2021, page 116. MIT Press One Rogers Street, Cambridge, MA 02142-1209, 2021.

[45] Eyvind Niklasson, Alexander Mordvintsev, Ettore Randazzo, and Michael Levin. Self-organising textures. *Distill*, 6(2):e00027–003, 2021.

[46] Maximilian Otte, Quentin Delfosse, Johannes Czech, and Kristian Kersting. Generative adversarial neural cellular automata. *arXiv preprint arXiv:2108.04328*, 2021.

[47] Ehsan Pajouheshgar, Yitao Xu, Tong Zhang, and Sabine Süsstrunk. Dynca: Real-time dynamic texture synthesis using neural cellular automata. In *Proceedings of the IEEE/CVF Conference on Computer Vision and Pattern Recognition*, pages 20742–20751, 2023.

[48] Ehsan Pajouheshgar, Yitao Xu, Alexander Mordvintsev, Eyvind Niklasson, Tong Zhang, and Sabine Süsstrunk. Mesh neural cellular automata. *ACM Trans. Graph.*, 2024. doi: 10.1145/3658127. URL <https://doi.org/10.1145/3658127>.

[49] Ehsan Pajouheshgar, Yitao Xu, and Sabine Süsstrunk. Noisenca: Noisy seed improves spatio-temporal continuity of neural cellular automata. *arXiv preprint arXiv:2404.06279*, 2024.

[50] Rasmus Berg Palm, Miguel Gonzalez Duque, Shyam Sudhakaran, and Sebastian Risi. Variational neural cellular automata. In *International Conference on Learning Representations 2022*, 2022.

[51] Zhiliang Peng, Wei Huang, Shanzhi Gu, Lingxi Xie, Yaowei Wang, Jianbin Jiao, and Qixiang Ye. Conformer: Local features coupling global representations for visual recognition. In *Proceedings of the IEEE/CVF International Conference on Computer Vision*, pages 367–376, 2021.

[52] Xinkuan Qiu, Meina Kan, Yongbin Zhou, Yanchao Bi, and Shiguang Shan. Shape-biased cnns are not always superior in out-of-distribution robustness. In *Proceedings of the IEEE/CVF Winter Conference on Applications of Computer Vision*, pages 2326–2335, 2024.

[53] Prajit Ramachandran, Niki Parmar, Ashish Vaswani, Irwan Bello, Anselm Levskaya, and Jon Shlens. Stand-alone self-attention in vision models. *Advances in Neural Information Processing Systems*, 32, 2019.

[54] Ettore Randazzo, Alexander Mordvintsev, Eyyvind Niklasson, Michael Levin, and Sam Greydanus. Self-classifying mnist digits. *Distill*, 2020. doi: 10.23915/distill.00027.002. <https://distill.pub/2020/selforg/mnist>.

[55] Olga Russakovsky, Jia Deng, Hao Su, Jonathan Krause, Sanjeev Satheesh, Sean Ma, Zhiheng Huang, Andrej Karpathy, Aditya Khosla, Michael Bernstein, et al. Imagenet large scale visual recognition challenge. *International journal of computer vision*, 115:211–252, 2015.

[56] Mark Sandler, Andrey Zhmoginov, Liangcheng Luo, Alexander Mordvintsev, Ettore Randazzo, et al. Image segmentation via cellular automata. *arXiv preprint arXiv:2008.04965*, 2020.

[57] Baifeng Shi, Yale Song, Neel Joshi, Trevor Darrell, and Xin Wang. Visual attention emerges from recurrent sparse reconstruction. In *International Conference on Machine Learning*, pages 20041–20056. PMLR, 2022.

[58] Nitish Srivastava, Geoffrey Hinton, Alex Krizhevsky, Ilya Sutskever, and Ruslan Salakhutdinov. Dropout: a simple way to prevent neural networks from overfitting. *The Journal of Machine Learning Research*, 15(1):1929–1958, 2014.

[59] Ajay Subramanian, Elena Sizikova, Najib Majaj, and Denis Pelli. Spatial-frequency channels, shape bias, and adversarial robustness. *Advances in Neural Information Processing Systems*, 36, 2024.

[60] Christian Szegedy, Wojciech Zaremba, Ilya Sutskever, Joan Bruna, Dumitru Erhan, Ian Goodfellow, and Rob Fergus. Intriguing properties of neural networks. In *2nd International Conference on Learning Representations, ICLR 2014*, 2014.

[61] Mattie Tesfaldet, Derek Nowrouzezahrai, and Chris Pal. Attention-based neural cellular automata. *Advances in Neural Information Processing Systems*, 35:8174–8186, 2022.

[62] Hugo Touvron, Matthieu Cord, Matthijs Douze, Francisco Massa, Alexandre Sablayrolles, and Hervé Jégou. Training data-efficient image transformers & distillation through attention. In *International Conference on Machine Learning*, pages 10347–10357. PMLR, 2021.

[63] Ashish Vaswani, Noam Shazeer, Niki Parmar, Jakob Uszkoreit, Llion Jones, Aidan N Gomez, Łukasz Kaiser, and Illia Polosukhin. Attention is all you need. *Advances in Neural Information Processing Systems*, 30, 2017.

[64] Ashish Vaswani, Prajit Ramachandran, Aravind Srinivas, Niki Parmar, Blake Hechtman, and Jonathon Shlens. Scaling local self-attention for parameter efficient visual backbones. In *Proceedings of the IEEE/CVF Conference on Computer Vision and Pattern Recognition*, pages 12894–12904, 2021.

[65] vtddggg. Code repo for: Rvt: Towards robust vision transformer. <https://github.com/vtddggg/Robust-Vision-Transformer>, 2021.

[66] Haohan Wang, Songwei Ge, Zachary Lipton, and Eric P Xing. Learning robust global representations by penalizing local predictive power. *Advances in Neural Information Processing Systems*, 32, 2019.

[67] Yujing Wang, Yaming Yang, Jiangang Bai, Mingliang Zhang, Jing Bai, Jing Yu, Ce Zhang, Gao Huang, and Yunhai Tong. Evolving attention with residual convolutions. In *International Conference on Machine Learning*, pages 10971–10980. PMLR, 2021.

[68] Ross Wightman. Pytorch image models. <https://github.com/rwightman/pytorch-image-models>, 2019.

[69] Haiping Wu, Bin Xiao, Noel Codella, Mengchen Liu, Xiyang Dai, Lu Yuan, and Lei Zhang. Cvt: Introducing convolutions to vision transformers. In *Proceedings of the IEEE/CVF International Conference on Computer Vision*, pages 22–31, 2021.

[70] Tete Xiao, Mannat Singh, Eric Mintun, Trevor Darrell, Piotr Dollár, and Ross Girshick. Early convolutions help transformers see better. *Advances in Neural Information Processing Systems*, 34:30392–30400, 2021.

[71] Shipeng Yan, Jiangwei Xie, and Xuming He. Der: Dynamically expandable representation for class incremental learning. In *Proceedings of the IEEE/CVF Conference on Computer Vision and Pattern Recognition*, pages 3014–3023, 2021.

[72] Jianwei Yang, Chunyuan Li, Pengchuan Zhang, Xiyang Dai, Bin Xiao, Lu Yuan, and Jianfeng Gao. Focal attention for long-range interactions in vision transformers. In M. Ranzato, A. Beygelzimer, Y. Dauphin, P.S. Liang, and J. Wortman Vaughan, editors, *Advances in Neural Information Processing Systems*, volume 34, pages 30008–30022. Curran Associates, Inc., 2021. URL [https://proceedings.neurips.cc/paper\\_files/paper/2021/file/fc1a36821b02abbd2503fd949bfc9131-Paper.pdf](https://proceedings.neurips.cc/paper_files/paper/2021/file/fc1a36821b02abbd2503fd949bfc9131-Paper.pdf).

[73] Tan Yu, Xu Li, Yunfeng Cai, Mingming Sun, and Ping Li. S2-mlp: Spatial-shift mlp architecture for vision. In *Proceedings of the IEEE/CVF Winter Conference on Applications of Computer Vision*, pages 297–306, 2022.

[74] Kun Yuan, Shaopeng Guo, Ziwei Liu, Aojun Zhou, Fengwei Yu, and Wei Wu. Incorporating convolution designs into visual transformers. In *Proceedings of the IEEE/CVF International Conference on Computer Vision*, pages 579–588, 2021.

[75] Li Yuan, Yunpeng Chen, Tao Wang, Weihao Yu, Yujun Shi, Zi-Hang Jiang, Francis EH Tay, Jiashi Feng, and Shuicheng Yan. Tokens-to-token vit: Training vision transformers from scratch on imagenet. In *Proceedings of the IEEE/CVF International Conference on Computer Vision*, pages 558–567, 2021.

[76] Xiaohua Zhai, Alexander Kolesnikov, Neil Houlsby, and Lucas Beyer. Scaling vision transformers. In *Proceedings of the IEEE/CVF Conference on Computer Vision and Pattern Recognition*, pages 12104–12113, 2022.

[77] Daquan Zhou, Zhiding Yu, Enze Xie, Chaowei Xiao, Animashree Anandkumar, Jiashi Feng, and Jose M Alvarez. Understanding the robustness in vision transformers. In *International Conference on Machine Learning*, pages 27378–27394. PMLR, 2022.

## Appendix: Table of Contents

<b>A Establish the correlation between AdaNCA placement and robustness improvement</b>	<b>16</b>
A.1 Dynamic programming for AdaNCA placement . . . . .	17
<b>B Notes on statistical significance</b>	<b>17</b>
<b>C ImageNet1K experiments</b>	<b>19</b>
C.1 AdaNCA settings for each model . . . . .	19
C.2 Discussion on the model choices . . . . .	19
C.3 Discussion on the hyperparameters of MLP inside AdaNCA . . . . .	19
C.4 The effect of AdaNCA placement on robustness on ImageNet1K . . . . .	20
C.5 Details of architecture change in Swin-Base* and ConViT-Base* . . . . .	20
C.6 Training details . . . . .	20
C.7 Adversarial attacks . . . . .	21
C.7.1 Choice of adversarial attacks . . . . .	21
C.7.2 Black-box attack . . . . .	21
C.8 Reason for using ImageNet22K model for RVT . . . . .	22
C.9 Visualization of attention maps . . . . .	22
C.10 Additional results on same model architecture but with more layers (★ models) . . . . .	22
C.11 Additional results on layer similarity structure . . . . .	24
C.12 Additional results on category-wise mCE on ImageNet-C . . . . .	24
C.13 Additional results on noise sensitivity examination . . . . .	25
C.14 Datasets information and license . . . . .	25
C.15 Model and code license . . . . .	26
<b>D Analysis on the efficiency improvement of AdaNCA</b>	<b>26</b>

	RVT-S-AdaNCA	FAN-S-AdaNCA	Swin-T-AdaNCA
Learning rate	2.5e-4	2.5e-4	2.5e-4
Batch size	256	256	256
Model EMA decay	0.99992	0.9999	/
Stochastic depth	0.1	0.25	0.1
Random erase prob	0.25	0.3	0.25
Gradient clip	None	None	5.0
MixUp	0.8	0.8	0.8
Label smoothing	0.1	0.1	0.1
Min learning rate	1e-5	1e-6	1e-5
Weight decay	0.05	0.05	0.05

Table 4: Hyperparameters used in AdaNCA-equipped ViT training for analysis in Section 3.3 on ImageNet100.

	PGD [40]	CW [5]	APGD-DLR [9]	APGD-CE [9]
Max magnitude	0.5	/	0.5	0.5
Steps	5	20	5	5
Step size	0.25	/	/	/
$\kappa$	/	0.0	/	/
$c$	/	0.25	/	/
$\rho$	/	/	0.75	0.75
EoT	/	/	1	1

Table 5: Hyperparameters in different adversarial attacks used in the analysis in Section 3.3 on ImageNet100 as well as our ablation studies.

## A Establish the correlation between AdaNCA placement and robustness improvement

Our motivation for investigating the relationship between AdaNCA and robustness stems from an empirical observation, namely that making neural networks more monolithic contributes to their robustness [27]. One of these monolithic ideas is redundancy in networks. It has been observed that several consecutive layers output similar results [4], hence building what we call “a layer set.” We hypothesize that AdaNCA, as adaptors inside ViTs, should connect the different sets inside a ViT and transmit information between them. In this way, layers inside a set will no longer bother adapting to other layers outside the set, improving the redundancy and thus robustness. To this end, we propose the layer redundancy quantification  $\kappa$  and network redundancy quantification  $\mathcal{K}$ , as well as the robustness improvement measurement  $\gamma$  in Section 3.3.

For the robustness improvement, we insert AdaNCA into all possible positions of 3 ViT models, Swin-tiny [37], FAN-small-hybrid [77], and RVT-small-plus [41], and train them along with the baseline models on the ImageNet100 dataset [15, 71, 73], a representative 100-class subset of ImageNet1K. The total amount of models is 34, including 3 baselines and 31 AdaNCA models. All AdaNCA-models have a 1%-2% parameter increase and 5% more FLOPs. The training hyperparameters are given in Table 4. All models are trained for 300 epochs with the Cosine scheduler. Here, we only consider adversarial robustness for simplification, as it is shown that adversarial robustness is correlated with image corruption robustness within one backbone architecture [41]. We use a white-box version of AutoAttack [9] in the AdaNCA placement analysis in Section 3.3, which comprises PGD [40], CW [5], APGD-DLR [9], and APGD-CE [9]. The hyperparameters of the four attacks are in Table 5.

We show the qualitative results of our experiments on the Set Cohesion Index and robustness improvement in Figure 7 and the quantitative results in Figure 8. Qualitatively,  $\gamma$  generally follows the trend of  $\mathcal{K}$  except for the top 3 layers and the last layer. Specifically,  $\gamma$  for the top three layers consistently exhibits a pattern where it decreases in the second layer and increases in the third layer, regardless of the trend in  $\mathcal{K}$ , which always increases. We hypothesize that the proximity of the top 3 layers to the input image causes AdaNCA to similarly impact the model’s robustness by adapting the

input to the subsequent layers. Furthermore, the position immediately before the final layer likely serves as a transitional stage for output, adapting to different output strategies (e.g., FAN has an additional class attention head while Swin and RVT use average pooling on all tokens to generate features for classification). The distinct behavior of the last layer compared to other layers has also been noted in previous research [20]. Hence, we exclude the models (AdaNCA applied in the top three layers and before the final layer) from our analysis. The resulting number of models is 19. To conduct a cross-model quantitative comparison, we normalize all  $\gamma$  as well as all  $\mathcal{K}$  in a single type of model. Each of the 3 models thus has a set of  $\gamma_{norm} \in [0, 1]$  as well as  $\mathcal{K}_{norm} \in [0, 1]$ . We plot all sets of  $\gamma_{norm}$  and  $\mathcal{K}_{norm}$  from 3 models in Figure 8. Note that the coordinate (1.0, 1.0) has two overlapping points (Swin-tiny and FAN-small-hybrid), hence only 18 points are visible in the figure.  $\gamma_{norm}$  is significantly correlated with  $\mathcal{K}_{norm}$  ( $r = 0.6938, p = 9.8e - 4$ ), as we report in Section 3.3.

### A.1 Dynamic programming for AdaNCA placement

Given  $\mathcal{U}$  AdaNCAs, the ViT is expected to be partitioned into  $\mathcal{U} + 1$  sets. The dynamic programming involves filling an array  $\mathcal{D}$ , where  $\mathcal{D}[i][u]$  represent the maximum value of  $\mathcal{K}$  achievable by partitioning the first  $i$  layers into  $u$  sets. The  $\mathcal{D}$  can be obtained via Equation 11.

$$\mathcal{D}[i][u] = \max_{j < i} (\mathcal{D}[j][u-1] + \kappa(j, i-1)) \quad (11)$$

The boundary conditions are: 1)  $\mathcal{D}[i][1] = \kappa(1, i)$ , which is partitioning the first  $i$  layers into 1 set; 2)  $\mathcal{D}[0][u] = 0$ . By recording the partition position, we can find  $\mathcal{U}$  partition points for inserting the AdaNCA. The pseudo-code is presented in Algorithm 1.

---

#### Algorithm 1 find\_optimal\_partition(Similarity Matrix $S$ , Number of Stages $\mathcal{U}$ )

---

```

1:  $n \leftarrow$  length of  $S$ 
2: Initialize dp with dimensions  $(n + 1, \mathcal{U} + 1)$ , filled with  $-\infty$ 
3: Initialize partition with dimensions  $(n + 1, \mathcal{U} + 1)$ , filled with zeros
4: dp[0][0]  $\leftarrow 0$  {Base case}
5: for each  $i$  from 1 to  $n$  do
6:   for each  $u$  from 1 to  $\min(i, \mathcal{U})$  do
7:     for each  $j$  from 0 to  $i - 1$  do
8:       current_value  $\leftarrow$  dp[j][u-1] +  $\kappa(j, i-1)$ 
9:       if current_value  $>$  dp[i][u] then
10:         dp[i][u]  $\leftarrow$  current_value
11:         partition[i][u]  $\leftarrow j$ 
12:       end if
13:     end for
14:   end for
15: end for
16: Initialize stages as an empty list
17: current_layer  $\leftarrow n$ 
18: current_stage  $\leftarrow \mathcal{U}$ 
19: while current_stage  $> 0$  do
20:   start_layer  $\leftarrow$  partition[current_layer][current_stage] + 1
21:   Append (start_layer, current_layer) to stages
22:   current_layer  $\leftarrow$  partition[current_layer][current_stage]
23:   current_stage  $\leftarrow$  current_stage - 1
24: end while
25: stages = stages[::-1]
26: return stages

```

---

Note that here the layer index starts from 0, and so does the input requirement of  $\kappa$ .

### B Notes on statistical significance

We do not report the error bar for training models with different seeds on ImageNet1K, as it would be very expensive (Table 9). However, we follow the seed used in the released code for each model. We

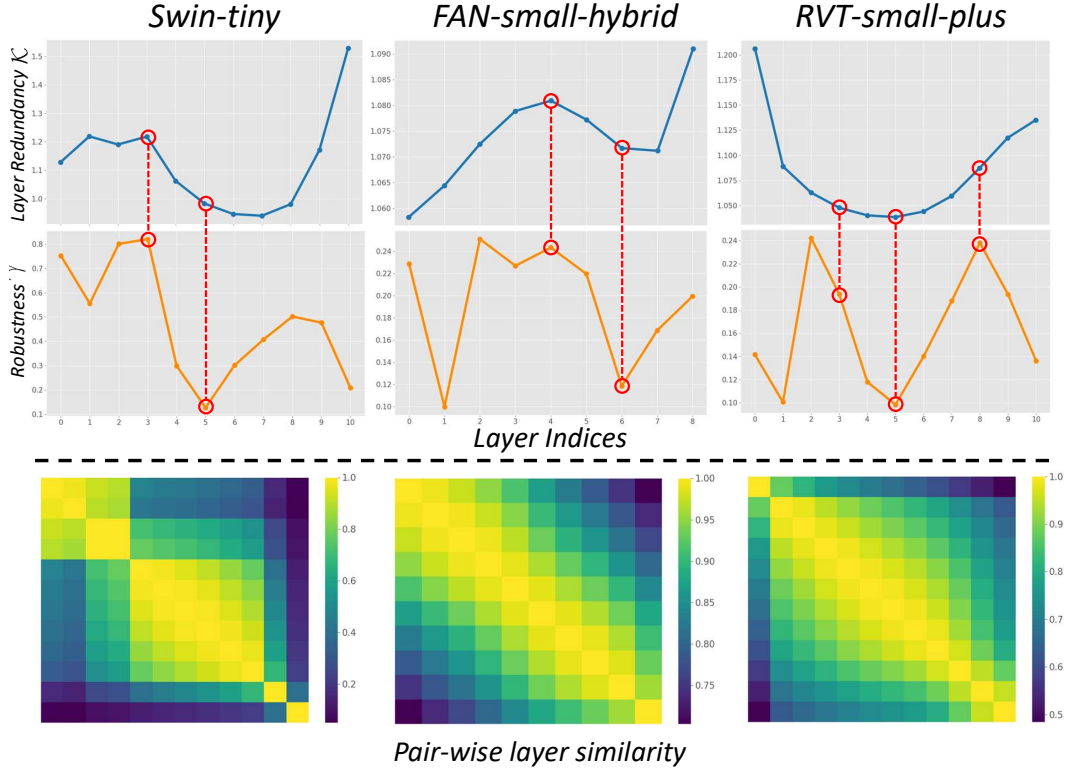


Figure 7: Top: Visualization of layer redundancy ( $\mathcal{K}(i) = \kappa(1, i+1) + \kappa(i+2, L)$ ) and corresponding robustness improvement  $\gamma$ . Bottom: Visualization of pair-wise layer similarity of the 3 ViTs.

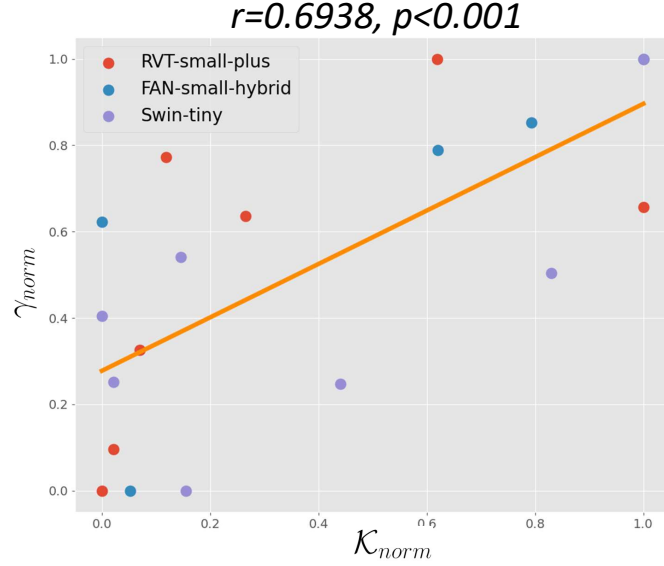


Figure 8: The relationship between the layer redundancy  $\mathcal{K}$  and robustness improvement  $\gamma$  by inserting AdaNCA in the corresponding position.  $\gamma_{norm}$  and  $\mathcal{K}_{norm}$  are obtained by normalizing  $\gamma$  and  $\mathcal{K}$  within the results of each model. Note that the coordinate (1.0,1.0) has two overlapping points (Swin-tiny and FAN-small-hybrid). Quantitatively,  $\gamma_{norm}$  is significantly correlated with  $\mathcal{K}_{norm}$  ( $r = 0.6938, p < 0.001$ ). The linear fit is shown in orange.

Table 6: AdaNCA settings for each ViT.

	# Layers	AdaNCA positions (after the index)	Training steps	Test steps	Stochastic update
RVT-B-AdaNCA	12	4,8	[2,4],[3,5]	3,3	0.1
FAN-B-AdaNCA	16	0,6,9	[2,2],[3,5],[2,4]	2,4,3	0.1
Swin-B-AdaNCA	24	2,8,22	[2,2],[3,5],[2,4]	2,4,3	0.1
ConViT-B-AdaNCA	12	5,9	[3,5],[2,4]	3,3	0.1

test the adversarial attack using 5 seeds and find the difference between different seeds negligible (standard deviation: PGD 0.08, CW 0.01, APGD-DLR 0.01, APGD-CE 0.02). As all our results on adversarial attacks have differences larger than 0.1, they are statistically significant.

For ImageNet100 experiments in the ablation study, we train the model 3 times and find the clean accuracy changes within a small range (standard deviation 0.08), and the robustness test results barely change (standard deviation 0.02). We also test the robustness improvement within one model using 5 seeds and the standard deviation is 0.008.

For the AdaNCA placement analysis, our correlation result is statistically significant ( $p < 0.001$ ).

## C ImageNet1K experiments

### C.1 AdaNCA settings for each model

Based on Algorithm 1, we insert AdaNCA into the four chosen baseline models. The specific settings for each AdaNCA are shown in Table 6. Note that insert position 0 means before the network, since FAN-B model uses a complex patch embedding layer, we can treat it as a unique layer that encodes semantic information rather than the simple convolution patch embedding used in other models. In practice, we find inserting AdaNCA after it can contribute to the model performance. Moreover, we add the drop path operation after each AdaNCA, and the drop path rate follows the one of the layer that AdaNCA follows. Hence, the regularization is pretty strong even without the stochastic update. However, as shown in our ablation studies in Section 4.3, the stochastic update indeed contributes to the model performance. Our FLOPs computation for AdaNCA models are based on Test steps.

### C.2 Discussion on the model choices

In our experiments, we choose RVT [41], FAN [77], Swin [37], and ConViT [16]. Our choice not only includes different types of ViTs (Regular, Hybrid, Hierarchical) and robust as well as non-robust architectures (RVT, FAN and Swin, ConViT), but also covers other aspects of ViT characteristics. First, RVT and Swin use average pooling on the final token maps to obtain the 1D feature for classification, while FAN and ConViT adopt a separate class token. It has been proved that those two strategies of classification can have a significant influence on the model robustness [41]. Despite this, AdaNCA are effective in both ways for classification. Moreover, all the architectures already contain certain kinds of local structures. RVT contains depth-wise convolution within MLP and a convolutional patch embedding layer. FAN has a ConvNeXt [39] head for patch embedding. Swin has shifted window attention. ConViT has convolution-attention coupled gated positional self-attention layers. Local structures have been proven effective in improving model robustness [41]. Therefore, we partially eliminate the possibility that AdaNCA is effective simply because of introducing local information in ViTs without any local inductive bias, such as the original ViT [14] or DeiT [62]. As shown in our ablation studies in Section 4.3, AdaNCA not only contributes to more parameter-efficient models but also improves the model robustness compared to not using the training strategies or design from NCA. Furthermore, in our choices, Swin does not conduct weight exponential moving average (EMA), while the other 3 models perform. It indicates that AdaNCA can be effective with or without model EMA.

### C.3 Discussion on the hyperparameters of MLP inside AdaNCA

In AdaNCA, we set the hidden dimensionality of the MLP to the same one as the input dimension. It is different from the common design choice of MLP in ViT that uses a 4-time larger hidden layer

Table 7: Comparison between different schemes of AdaNCA placement. **No-Prior**: insert AdaNCA without knowledge of layer similarity structure but making the most reasonable choice, that is to insert them between the architectural stage transition where the embedding dimensionality changes for Hierarchical ViT like Swin [37], or insert them uniformly between layers that have the same structure like the main network in FAN [77]. AdaNCA consistently improves the model performance and robustness compared to the baseline models, while the improvement can be maximized by using our AdaNCA placement scheme based on Algorithm 1.

Model	Insert Scheme	Params (M)	FLOPs (G)	ImageNet Top-1	Robustness Benchmarks							
					PGD	CW	APGD-DLR	APGD-CE	IM-C (.)	IM-A	IM-R	IM-SK
Swin-B [37]	/	87.8	15.4	83.4	21.3	13.4	15.6	23.1	54.2	35.8	46.6	32.4
Swin-B-AdaNCA	No-Prior	90.7	16.3	83.6	23.1	19.4	24.8	24.5	52.0	<b>36.0</b>	47.7	34.8
Swin-B-AdaNCA	Ours	90.7	16.3	<b>83.7</b>	<b>24.1</b>	<b>20.5</b>	<b>25.1</b>	<b>24.8</b>	<b>51.5</b>	<b>36.0</b>	<b>48.2</b>	<b>35.5</b>
FAN-B [77]	/	50.4	11.7	83.9	15.0	7.6	10.4	13.1	46.1	39.6	52.7	40.8
FAN-B-AdaNCA	No-Prior	51.7	12.4	<b>84.1</b>	17.3	10.2	13.5	16.3	<b>44.7</b>	42.8	<b>53.5</b>	<b>41.0</b>
FAN-B-AdaNCA	Ours	51.7	12.4	<b>84.1</b>	<b>20.3</b>	<b>10.6</b>	<b>14.1</b>	<b>19.1</b>	<b>44.7</b>	<b>42.9</b>	53.4	<b>41.0</b>

than the input layer. Moreover, it also deviates from the design of the previous NCA that uses more than 8 times larger hidden layer size than the input one. Instead, we set the hidden dimensionality to be the same as the input one. The reason is that AdaNCA introduces additional parameters and computation in ViTs and we want the extra computational overhead to be as low as possible. The lowest dimensionality that will not cause inevitable information loss is the same one as the input dimension. Therefore, we design the MLP in AdaNCA as a non-compression-non-expand structure.

#### C.4 The effect of AdaNCA placement on robustness on ImageNet1K

Our algorithm for deciding the placement of AdaNCA is based on the correlation between the robustness improvement and the Set Cohesion Index in Section 3.3. All the experiments are conducted on ImageNet100 to efficiently use the computational resources. Here, we compare two schemes for deciding the placement of AdaNCA on ImageNet1K on Swin-B [37] and FAN-B [77] to demonstrate our result validity. The first scheme is **No-Prior**, which does not involve the knowledge of the layer similarity and performs the most reasonable placement choice. For Swin-B, the choice for placing 3 AdaNCA is to insert them between each stage pair defined by the transition between different embedding dimensionalities, namely after layer 2, layer 4, and layer 22. Coincidentally, this choice aligns with what we obtain from the dynamic programming algorithm, which is to place AdaNCA after layer 2, layer 8, and layer 22. For FAN-B, although it is a hybrid ViT, we only consider inserting AdaNCA into its main network where all layers share the same structure. In this case, the **No-Prior** chooses to uniformly insert AdaNCA between the 16 layers, that is after layers 5 and 10. Our algorithm decides the placement should instead be after layers 6 and 9. Table 7 shows the results of two Swin-B-AdaNCA models. Inserting AdaNCA with the **No-Prior** scheme can still contribute to the model performance and robustness, but not as effective as using our proposed method.

#### C.5 Details of architecture change in Swin-Base\* and ConViT-Base\*

For Swin-Base\*, we add two extra layers in stage 3 with embedding dimensionality being 512, since in the original design most of the computational budgets are dedicated to stage 3, and two layers form a complete Swin operation. For ConViT-Base\*, we add an extra Gated Positional Self-Attention (GPSA) layer.

#### C.6 Training details

We use different training schemes for the four selected baseline models, closely following the parameter settings for each of them (link to reference configuration files: **RVT-B**, **FAN-B**, **Swin-B**, **ConViT-B**). Most training settings are in line with DeiT [62] since all models used build the training upon the scheme of training a DeiT but with minor changes. Some specific training settings are listed in Table 8.

All models are trained for 300 epochs. Our ablation studies on the size of the model (Swin-B-abl, ConViT-B-abl) also follow the same training settings. The detailed time consumption for training

Table 8: Hyperparameters used in AdaNCA-equipped ViT training.

	RVT-B-AdaNCA	FAN-B-AdaNCA	Swin-B-AdaNCA	ConViT-B-AdaNCA
Learning rate	1e-3	2e-3	1e-3	1e-3
Batch size	1024	2048	1024	1024
Model EMA decay	0.99996	0.99992	/	0.99996
Stochastic depth	0.1	0.35	0.5	0.1
Random erase prob	0.25	0.3	0.25	0.25
Gradient clip	None	None	5.0	None
MixUp	0.8	0.8	0.8	0.8
Label smoothing	0.1	0.1	0.1	0.1
Min learning rate	1e-5	1e-6	1e-5	1e-5
Weight decay	0.05	0.05	0.05	0.05

Table 9: Training time of each AdaNCA-equipped ViT.

	RVT-B-AdaNCA	FAN-B-AdaNCA	Swin-B-AdaNCA	ConViT-B-AdaNCA
Training time (hours)	400	180	120	100

each model using 4 Nvidia-A100 80G GPUs is in Table 9. The excessive time of RVT is because of the patch-wise augmentation [41].

## C.7 Adversarial attacks

We test all AdaNCA-equipped ViTs using four adversarial attacks based on the code [33]. The detailed setting of each attack is given in Table 10. We try setting the Expectation Over Transformation (EOT) to 3 and the results do not change significantly (For Swin-B, APGD-DLR, EOT=1: 25.124, EOT=3: 25.121). Hence, we fix the EOT to 1.

### C.7.1 Choice of adversarial attacks

We choose PGD [40] since it is the most popular method for examining model adversarial robustness after architectural changes [57, 41]. However, it is relatively easy to overcome the PGD attack using obfuscated gradients through methods such as random inference, noisy architecture, or non-differentiable components [3]. Our AdaNCA does not fulfill the requirement for producing obfuscated gradients since it is fully differentiable and we turn off all randomness during test. However, we still want to examine whether recurrence would result in corrupted gradient information due to the drawback of cross entropy loss [9]. Moreover, the step size in PGD can largely affect the result. Hence, we choose Auto-PGD family [9] to automatically decide the step size and incorporate the new Difference of Logits Ratio (DLR) loss, resulting in APGD-CE and APGD-DLR, respectively. We also want to include an optimization-based adversarial attack and thus select the CW [5] attack.

### C.7.2 Black-box attack

We also consider the black-box attack, specifically Square [2]. However, due to the extreme computational cost of performing Square on ImageNet1K, we instead conduct Square attack to three

Table 10: Hyperparameters in different adversarial attacks.

	PGD [40]	CW [5]	APGD-DLR [9]	APGD-CE [9]
Max magnitude	1.0	/	1.0	1.0
Steps	5	20	5	5
Step size	0.5	/	/	/
$\kappa$	/	0.0	/	/
$c$	/	0.5	/	/
$\rho$	/	/	0.75	0.75
EOT	/	/	1	1

Table 11: Results of ViTs and AdaNCA models under Square [2] attack on ImageNet100.

	Placement (after)	Clean Acc.	Square	Attack Failure Rate
Swin-T [37]	/	86.56	16.18	18.69
Swin-T-AdaNCA	4	<b>87.18</b>	<b>31.74</b>	<b>36.41</b>
FAN-S [77]	/	87.30	29.44	33.72
FAN-S-AdaNCA	5	<b>88.22</b>	<b>42.24</b>	<b>47.88</b>
RVT-S [41]	/	87.18	33.14	38.01
RVT-S-AdaNCA	9	<b>87.50</b>	<b>39.12</b>	<b>44.71</b>

models, Swin-tiny (Swin-T) [37], FAN-small-hybrid (FAN-S) [77], and RVT-small-plus (RVT-S), on ImageNet100. The three models are used in our AdaNCA analysis in Section 3.3. The maximum magnitude  $\epsilon = 6/255$  and the number of queries is 1000. Results are shown in Table 11. The AdaNCA placements are in line with the highest robustness improvement placements demonstrated in Figure 7.

### C.8 Reason for using ImageNet22K model for RVT

We use the ImageNet22K-pretrained model for RVT-Base-plus in our main results. This is because we do not find an official release of the ImageNet1K-trained weights. Moreover, our trainable parameter count on the model in the released code differs from the one reported in the original paper (ours: 88.5M, in-paper: 91.8M) [41, 65]. Hence, self-training might deviate from the results in the official paper. We tried to contact the author for an ImageNet1K version of the model but did not succeed. We test the result of the released model (ImageNet22K version) on PGD attack and get an accuracy of 30.47. In the paper, the authors report this number to be 29.9 on the ImageNet1K model. Hence, we assume that the results of adversarial attacks can be used as a representative, though might be slightly optimistic. Importantly, **this does not falsify our claim that TAPADL modification undermines the adversarial robustness of RVT**, since TAPADL-RVT already falls short in PGD attack when compared to the ImageNet1K version of RVT-Base-plus. However, for the O.O.D test, ImageNet22K model can differ a lot from the ImageNet1K models, as most data would be counted as in-distribution w.r.t ImageNet22K. Therefore, we use the official values reported in the original paper [41] on those benchmarks. Moreover, for the comparison other than adversarial attacks, we use TAPADL-RVT [22] as a proxy of the RVT model.

### C.9 Visualization of attention maps

We aim to qualitatively show that AdaNCA helps ViTs perform correct classification when facing noise. Here, we use GradCAM++ [6] to visualize the attention map of Swin-Base [37] and Swin-B-AdaNCA on the clean images as well as images containing adversarial noise. We use APGD-DLR to generate the adversarial images. Results are shown in Figure 9. We can observe that AdaNCA-enhanced Swin model focuses more on the objects, while the baseline model attends to areas unrelated to the object on the images when facing adversarial noise.

### C.10 Additional results on same model architecture but with more layers (★ models)

Due to the computational cost of RVT [41] and FAN [77] (Table 9), we do not train them with more layers and thus do not have a ★ version of these two models. Instead, we train the smaller version of models on ImageNet100. We choose RVT-small-plus (RVT-S) and FAN-small-hybrid (FAN-S) as two baselines, which is in line with our other experiments on ImageNet100. We add one extra layer to RVT-small-plus and one extra layer to the FAN network in FAN-small-hybrid, resulting in RVT-S★ and FAN-S★. We compare it with our AdaNCA-equipped model where AdaNCA is after layer 9 in RVT-S and after layer 5 in the FAN-S, aligning with Table 11. We use the same AutoAttack as described in Section A to measure the robustness improvement and attack failure rate. Results are shown in Table 12. We can observe that the increase in the number of parameters and FLOPs does not account for the improvement in robustness.

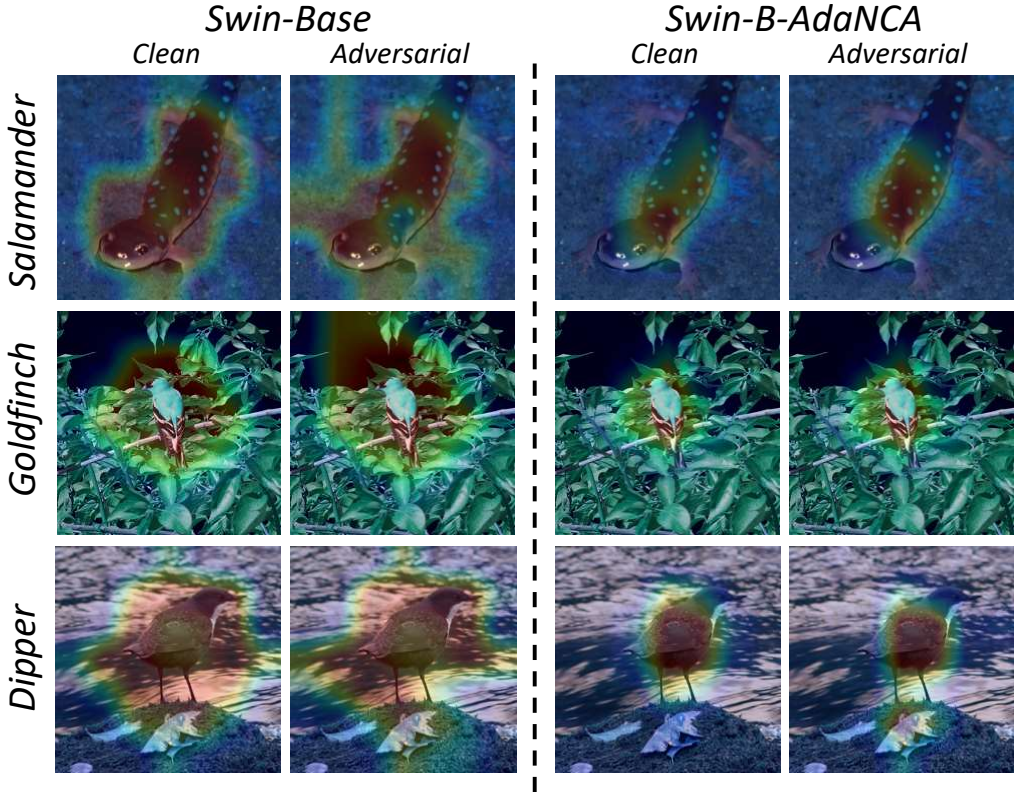


Figure 9: Visualization of attention maps of Swin-Base [37] and Swin-B-AdaNCA using GradCAM++ [6] on clean images and images with adversarial noise. AdaNCA helps ViTs focus more on the object when facing noise.

Table 12: Results of different ViTs on ImageNet100.  $\star$  means the same model design but with more layers. The improvement AdaNCA brings does not merely stem from the increase in the number of parameters or FLOPs.

	Params (M)	FLOPs (G)	Placement (after)	Clean Acc.	Acc. AutoAttack	Attack Failure Rate
FAN-S [77]	25.8	6.7	/	87.30	18.70	21.42
FAN-S $\star$ [77]	27.7	7.1	/	87.46	19.40	22.88
FAN-S-AdaNCA	26.1	6.9	5	<b>88.22</b>	<b>27.76</b>	<b>31.47</b>
RVT-S [41]	23.0	4.7	/	87.18	29.80	34.18
RVT-S $\star$ [41]	24.8	5.1	/	<b>87.52</b>	32.14	36.72
RVT-S-AdaNCA	23.3	4.9	9	87.50	<b>36.90</b>	<b>42.17</b>

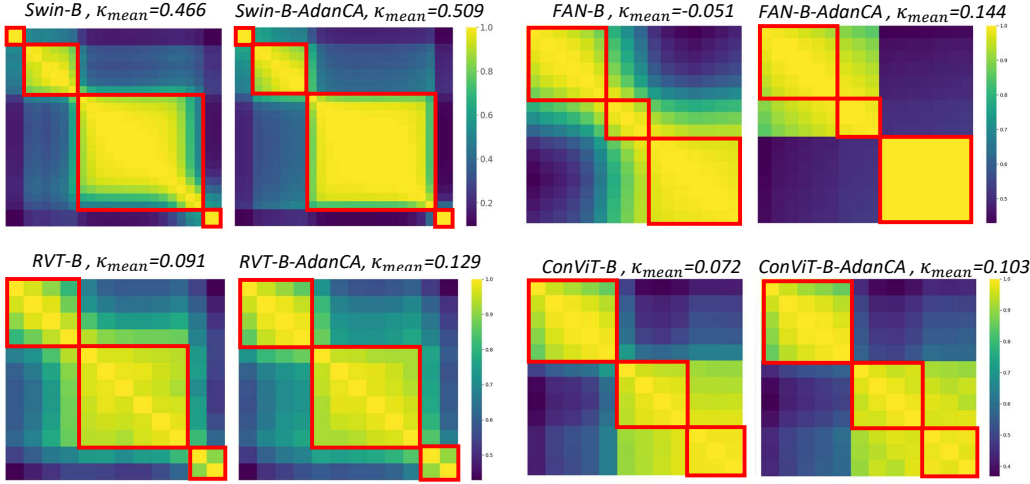


Figure 10: Layer similarity structures of different ViTs. Layer set marked in red boxes. AdaNCA is inserted between each pair of stages.  $\kappa_{mean}$  is the mean of  $\kappa$  of all stages marked out.

Table 13: Comparisons of corruption error on each corruption type of ImageNet-C. AdaNCA consistently improves the performance of different ViT models.

Model	mCE	Noise			Blur			Weather			Digital					
		Gauss	Shot	Impulse	Defocus	Glass	Motion	Zoom	Snow	Frost	Fog	Bright	Contrast	Elastic	Pixelate	JPEG
Swin-B [37]	54.3	43.8	45.7	43.8	61.6	73.2	55.5	66.5	50.0	47.4	47.9	42.1	38.7	68.8	66.4	62.6
Swin-B-AdaNCA	51.5	39.5	40.9	39.8	59.5	69.5	55.0	65.6	49.4	47.1	40.8	40.6	37.0	66.3	59.9	61.1
TAPADL-RVT [22]	44.7	34.6	36.1	34.0	53.9	62.3	52.2	60.1	41.9	44.9	35.8	37.4	31.9	57.1	41.1	47.2
RVT-B-AdaNCA	43.2	33.9	36.1	33.9	52.7	59.1	47.8	60.5	42.6	39.0	33.9	36.8	31.7	53.4	40.0	46.2
ConViT-B [16]	46.9	36.0	37.6	35.5	56.5	64.4	51.5	65.0	42.6	40.5	39.3	39.1	38.0	61.7	43.6	51.8
ConViT-B-AdaNCA	44.3	34.7	35.9	34.2	53.1	61.0	48.6	60.4	40.5	40.1	37.2	37.2	33.5	57.1	42.4	49.4
FAN-B [77]	46.1	36.5	36.8	34.7	52.8	65.9	47.7	56.9	40.6	44.4	37.9	37.4	34.3	62.8	52.8	50.6
FAN-B-AdaNCA	44.7	35.5	36.0	33.7	51.9	65.7	45.3	55.6	39.7	43.3	37.3	37.0	33.1	62.0	46.8	47.9

### C.11 Additional results on layer similarity structure

Here, we show the layer similarity structure for FAN-B-Hybrid [77] and ConViT-B [16] with the ImageNet1K weights and the weights after training with AdaNCA. For RVT-Base-plus, we train it with the released code [65] but with a different number of parameters, as discussed in Section C.8. This training is only for obtaining the layer similarity structure, and we find it stable after 30 epochs. The results are shown in Figure 10. In practice, we ignore the stage partition found by the dynamic programming algorithm in Section A.1 that is after the first layer or before the last layer since we want a stage to contain more than 1 layer. The results further validate our assumption that AdaNCA is used as an adaptor between stages and transmits information between them, making them more and more different from each other. Interestingly, not all AdaNCA contributes to drastic clearer stage partitions. For example, the first AdaNCA in FAN-B is not effective in making the stage as clear as the second one. However, the overall Set Cohesion Index increases, and the layer similarity structures in all 4 networks do not change. We believe the deep learning architecture research can benefit from our results, in that developing more architectural changes which contribute to stage partition in the network and examine the effect on network robustness and generalization. More importantly, we use a single non-parametric metric for quantifying the layer similarities. Introducing advanced output similarity quantification methods might lead to new findings and other fascinating results.

### C.12 Additional results on category-wise mCE on ImageNet-C

We provide additional results on category-wise mCE on ImageNet-C in Table 13. Our test follows the data transformation used in [41].

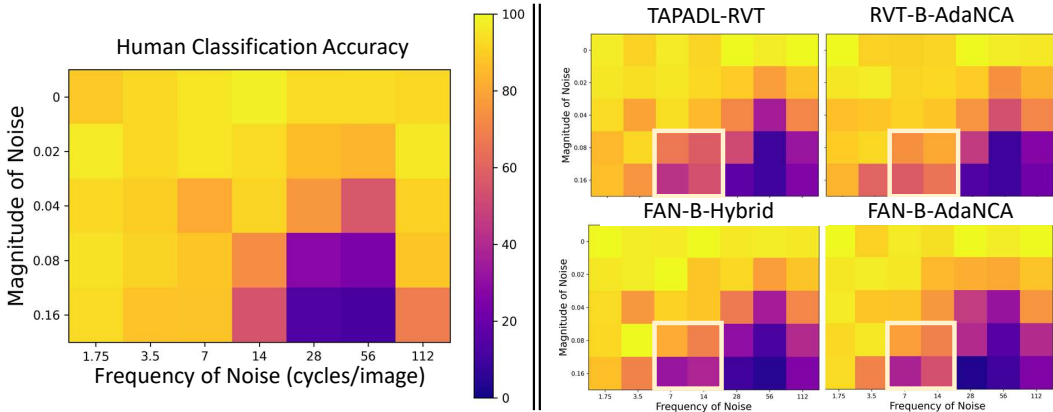


Figure 11: Noise sensitivity examination on humans and ViTs. AdaNCA contributes to more human-like noise-resilient ability and reduces the sensitivity of ViTs on certain types of noise (yellow boxes).

### C.13 Additional results on noise sensitivity examination

We use the data from [59]. In the experiment, human subjects are asked to classify the noise-contaminated images, and the classification accuracy is recorded. Then, the images are fed into the models trained on ImageNet1K, whose outputs are then transformed into a 16-way ImageNet label [55] and compared against the ground truth labels. Their classification accuracy is also recorded and used for comparison with human results. We present the additional results on FAN-B-Hybrid [77] and the SOTA model TAPADL-RVT [22] compared to the AdaNCA-equipped model in Figure 11.

Moreover, we adopt a quantitative metric on the test. In the original experiment [59], a Gaussian curve is fit based on the discretized accuracy map. However, such a method ignores the continuous change in the classification pattern. Hence, we propose a simple metric that examines the similarity between the accuracy map of humans and of models. Specifically, given the ground truth accuracy map (human performance)  $\mathcal{A}_{gt}$ , and model accuracy map  $\mathcal{A}_m$ , the similarity  $\Gamma$  is defined as:

$$\Gamma = 100 - \frac{1}{N} \sum_{\epsilon, f} |\mathcal{A}_m(\epsilon, f) - \mathcal{A}_{gt}(\epsilon, f)| \quad (12)$$

$\epsilon, f$  represent the magnitude and frequency of the noise, respectively. A higher  $\Gamma$  indicates that the model can achieve more similar accuracy maps with humans averaged across all noisy images.  $N$  is the total number of types of noise added. Since all models as well as humans perform similarly on low-magnitude noise, we ignore the first two noise levels ( $\epsilon = 0, 0.02$ ). Hence, in our experiments,  $N = 21$ . We report  $\Gamma$  in Table 14. We also include the results of ResNet50 [26] as well as the L2-adversarially-trained version [59] (ResNet50-Adv, trained with L2-bounded adversarial noise where the maximum magnitude of noise is 0.25), and present the visualizations of the accuracy maps of those two models in Figure. Critically, our results indicate that the adversarially trained model cannot lead to improved accuracy similarities, resulting in a less human-like noise-resilient ability. This is in line with the conclusion of the original work [59], validating our proposed metric. Contrary to adversarial training, we obtain more human-like decision patterns than the compared models, validating our claim in Section 4.4.

### C.14 Datasets information and license

- ImageNet1K [12]. This dataset contains 1.28M training images and 50000 images for validation. We report the top1 accuracy on the 50000 validation images. License: Custom (research, non-commercial).
- ImageNet-C [27]. This dataset contains 15 types of 2D image corruption types that are generated by different algorithms. The metric on this dataset is mean corruption error, whose lower value represents a more robust model against those corrupted images. License: CC BY 4.0.

Table 14: Quantitative results on the frequency preference examination experiments. We report the similarity of accuracy maps between model results and humans.

Accuracy map similarity to ground truth $\Gamma$	
ResNet50 [26]	72.23
ResNet50-Adv [59]	<b>52.12</b>
TAPADL-RVT [22]	81.91
RVT-B-AdaNCA	<b>82.17</b>
FAN-B-Hybrid [77]	83.52
FAN-B-AdaNCA	<b>84.75</b>
Swin-B [37]	77.07
Swin-B-AdaNCA	<b>81.34</b>
ConViT-B [16]	79.69
ConViT-B-AdaNCA	<b>81.56</b>

- ImageNet-A [13]. This dataset contains naturally existing adversarial examples that can drastically decrease the accuracy of ImageNet1K-trained CNNs. It is a 200-class subset of the ImageNet1K dataset. License: MIT license.
- ImageNet-R [29]. This dataset contains different artistic renditions of 200 classes from the original ImageNet object classes. The original ImageNet dataset discourages non-real-world images, and thus the artistic renditions render the images to be O.O.D. License: MIT license.
- ImageNet-SK [66]. This dataset contains 50000 images with 1000 classes that match the validation set of the original ImageNet dataset. All the images are black-and-white sketches instead of real-world photographs of the object class. License: MIT license.

### C.15 Model and code license

- Swin-B [37]: MIT License.
- FAN-B [77]: Nvidia Source Code License-NC.
- ConViT-B [16]: Apache 2.0 License.
- RVT [41]: Apache 2.0 License.
- TAPADL [22]: MIT License.
- Code for adversarial attacks [33]: MIT License.
- PyTorch Image Model [68]: Apache 2.0 License.
- Code for GradCAM++ [19]: MIT License.

## D Analysis on the efficiency improvement of AdaNCA

In our experiments, we do not conduct experiments on comparing the concatenation scheme and our weighted sum scheme in the *Interaction* stage. It is because the concatenation scheme will result in a huge increase in the number of parameters as well as FLOPs, rendering comparison unfair and making the source of performance improvement undecidable. Concretely, with both the token and hidden dimensions of the MLP set at  $C$ , the parameter count and FLOPs required to update a single token are nearly  $5C^2$ . For a standard base-level ViT configuration with  $C = 768$  and token number  $N = 196$ , this results in near  $0.6G$  FLOPs per iteration for a single NCA, and incorporating recurrence further increases the computational demands. If we adopt the concatenation scheme in the RVT-B-AdaNCA model, it will result in  $\sim 10M$  more parameters and  $\sim 4G$  more FLOPs during test. Hence, we decide not to include the comparison between the original *Interaction* scheme and our *Dynamic Interaction*. However, we do conduct an ablation in Section 4.3 on mean aggregation versus our weight sum scheme and demonstrate the effectiveness of our proposed *Dynamic Interaction* in improving model performance and robustness.